AN INVESTIGATION OF THE INTERFERENCE EFFECTS OF A STING SUPPORT SYSTEM ON THE PRESSURE DISTRIBUTION OVER A BODY OF REVOLUTION

Thesis by

Harris M. Schurmeier

In Partial Fulfillment of the Requirements

For the Degree of

Aeronautical Engineer

California Institute of Technology

Pasadena, California

1949

ABSTRACT

The pressure distribution over a body of revolution was measured, both with and without a sting, or sting and simulated sting-support structure, present. The investigation was carried out in a wind tunnel at a low speed.

The results indicated that the changes in the pressure distribution over the body were small if the sting diameter was half the base diameter and the sting made reasonably long. The effects of the sting and sting-support structure were felt only over the aft 20 percent of the body and were such as to increase the pressure in all cases investigated.

ACKNOWLEDGEMENTS

The author wishes to express his thanks and appreciation to Mr. R.W.Bell, under whose direction this investigation was conducted and to Dr. C.B.Millikan and J.E.Smith for their technical advice.

The author also wishes to thank Elmer Ward for his work on the mechanical design of the model and Bettye Jo Parris for her work on the figures and manuscript.

TABLE OF CONTENTS

Index of Figures

Index of Figures (Cont'd)

Index of Figures (Cont'd)

Index of Model Photos

Photo No.

1. Lower-front view of configuration B showing the model installed in the tunnel.
2. Side view of configuration B.
3. Rear view of configuration B_1.
4. Rear-side view of configuration $B_1 + S_1$.
5. Rear-side view of configuration B_2 showing base pressure orifices.
6. Rear-side view of configuration $B_2 + S_1$.
7. Side view of configuration $B_2 + S_1 + P_4$ showing pod.
8. Side view of configuration $B_2 + S_1 + Strut_{12}$ showing dummy strut.
9. Side view of configuration $B_2 + S_2$ showing the effective infinite sting.
10. Rear view of configuration B_4 showing base pressure orifices.
11. Rear view of configuration $B_4 + S_2$.
12. Configuration $B_1 + S_1$ showing removable aft sections.
13. Photo showing the pressure leads inside the fuselage.

Test Notation*

R = Reynolds number = $\frac{\rho d V}{\mu}$

q = Tunnel free stream dynamic pressure = $\frac{\rho V^2}{2}$

ρ = Mass density of air

d = Maximum diameter of body in inches

V = Average wind velocity

μ = Absolute viscosity $\doteq 3.93 \times 10^{-7} \left(\frac{T}{308}\right)^{0.78} \frac{\text{lbwt sec}}{\text{ft}^2}$

T = Temperature in degrees Kelvin of the equivalent free air stream

α = Angle of attack of the fuselage reference line relative to the effective zero angle of attack (cf. Section III). (Angular displacements are positive when the nose is raised, trailing edge lowered.)

x = Distance, in inches, aft of the nose of the model, measured along the axis of the fuselage.

r = Radius, in inches, measured on the base of the body

θ = Polar angle measured clockwise from the lower vertical in a plane perpendicular to the axis of the fuselage.

$\frac{p}{q} = \frac{P - P_{\mathbb{Q}}}{q}$ = Static-pressure coefficient

P = Measured static pressure

$P_{\mathbb{Q}}$ = Tunnel free stream static pressure measured on the tunnel axis at the centerline of the test section.

* All angular displacements are defined with respect to the pilot

Model Configuration Notation*

B = Basic clean configuration; fuselage with the tail faired to a pointed end.

B_a = Basic clean configuration cut off. The subscript "a" denotes the base diameter, in inches, which is the diameter at the cut.

S_b = Dummy sting. The subscript "b" denotes the diameter of the sting, in inches.

P_y = Pod used to vary the effective length of the one-inch sting. The subscript "y" denotes the distance downstream, in inches, from the base of the fuselage to the leading edge of the pod.

$Strut_y$ = Dummy strut used to vary the effective length of the one-inch sting. The subscript "y" denotes the distance downstream, in inches, from the base of the fuselage to the leading edge of the strut.

* Numbers of the Model drawings on file at the GALCIT are: 3-284-5, 5-284-6, 4-284-7, 4-284-8, 4-284-9, 2-284-10, 2-284-11, 3-284-12, 3-284-13.

Model Dimensional Data

A. Body

	B	B_1	B_2	B_4
Length, inches	72.00	70.34	68.56	64.66
Base diameter, inches		1.00	2.00	4.00
Diameter (maximum), inches	8.00	8.00	8.00	8.00
Cross sectional area (maximum), inches^2	50.27	50.27	50.27	50.27

B. Wing (all configurations)

Span, inches	60.00
Chord, inches	15.13
Area*, inches^2	907.8

C. Sting

	S_1	S_2
Length**, inches	38.00	41.00
Tail fairing length, inches	3.00	6.00
Diameter, inches	1.00	2.00

* Includes area covered by fuselage

** Sting length includes tail fairing

I. Introduction

The emphasis on high-speed wind-tunnel testing has increased in the past several years, and simultaneously the problem of supporting a model so that the support structure affects the flow over the model as little as possible has become a critical one, especially at high subsonic Mach numbers. A model, such as a stub-winged missile, supported by the conventional three-strut type of support, or even by a single swept strut, gives unsatisfactory results at high Mach numbers because of the interference and blockage effects of the struts. These effects are large and in many cases most difficult to evaluate.

One method of support coming more into use is the sting mount, by which the model is supported on a tube that enters the model at the tail. In this system the entire supporting structure is downstream of the model. If the sting is made sufficiently long, the structure supporting it will have little or no effect on the model. When this type of support is employed, the balance system is usually contained within the model, and the only forces measured are those acting upon the model itself. However, these measured forces still differ from the true model forces by the amount of the interference from the sting and its support. Sting mounting minimizes but does not necessarily eliminate support interference effects.

The problem has therefore arisen of determining interference effects for sting-mounted models. The analytical approach to this problem, if plausible, appears to be extremely complicated and laborious. Since the characteristics of the interference are not well known or understood, it was thought advisable to investigate them experimentally and, for simplicity, to carry out the first investigation in the low speed range. The present investigation is an attempt to establish the magnitudes of the interference effects and to determine to what extent they affect the pressure distribution over the model.

Introduction (Cont'd)

As simple a configuration as was possible to build was used to determine the fundamental parameters of these interference effects. It was felt that two basic parameters were the ratio of model base diameter to sting diameter and, the length of the sting between the model and the sting support structure. In addition, it was desirable to investigate the changes in the pressure distribution over a basically point-ended body when the tail is cut off to provide entry for the sting. The model was designed to allow variation of all three of these parameters.

The test facilities limited the investigation to a dynamic pressure of 60 psf, and the limited tunnel time available rendered the investigation far from complete. However it was possible to obtain data for one body of revolution with three base diameters, tested in conjunction with two stings of different diameters. Data were also obtained for various effective sting lengths. Results of these investigations, conducted from April 26 to May 3, 1949, are presented in this report.

II. Experimental Equipment

The tests were conducted in the GALCIT ten-foot Wind Tunnel. The experimental configuration was a body of revolution mounted symmetrically on a constant-chord, symmetrical-profile wing. The model was centrally mounted in the tunnel with the main struts placed near the wing tips (cf. Fig.1). In place of the regular tail strut that normally extends into the aft portion of the fuselage, a short sting was fastened to each wing tip just inboard of the main trunnion fitting, and extended downstream 20 inches from the wing trailing edge. A one-inch diameter rod was pinned to the end of each sting and, extending vertically downward through the tunnel floor, was connected to the tail image-windshield mount through a whiffle-tree. The tail image-windshield drive was used to vary the angle of attack of the model. The main image-windshields were installed to retain as symmetrical mounting conditions as possible.

This experimental-model configuration and type of mounting were selected as being the best all around choice from the standpoint of cost and practicability. The major problem was to remove struts and windshields as far as possible from the body of revolution because of their large interference effects. The wing was used as a method of supporting the body and as a means of getting the pressure leads out of the body. Although the problem of wing-interference effects still remained, it was felt that this configuration was representative of an airplane or stub-winged missile.

The pressure leads were taken out through the wing tips, down inside the main image-windshields, to two multiple tube manometers situated on the floor below the test section. The manometers were filled with alcohol and the fluid heights recorded photographically.

The size and contour of the body of revolution were chosen to give optimum results from two basic considerations. First, it was desirable that the body be representative of a high-speed airplane fuselage or missile. This required that the fineness ratio lie in the range, eight to twelve.

Experimental Equipment (Cont'd)

Second, it was required that the body be a practical experimental model. This second consideration involved such details as the locations and size of orifices, and the facility with which the model could be constructed and test configurations changed.

The fuselage, 72 inches long and 8 inches maximum diameter, was designed with the upper center section and aft portions removable. The removable upper section was necessary in order to make pressure tube connections for each model configuration; the removable aft portions enabled the base diameter to be varied. The fuselage was constructed with four removable aft sections so that base diameters of one inch, two inches, four inches and six inches could be used. The fixed part, removable center portion, and the largest removable aft section of the fuselage were made of laminated mahogany. The three smaller aft sections were turned from brass. The details of the model construction are shown by Photos 12 and 13 (see page 6 for the numbers of the model drawings on file at the GALCIT).

The static pressure orifices were made by installing 1/16 inch o.d., thin-walled, copper tubing with the ends flush with the surface. This made orifices of approximately 1/32 in diameter. Most of the orifices were located in the lower left surface between the horizontal and vertical planes of symmetry (looking forward); a few check orifices were located on the top and right sides of the fuselage (see Fig. 2). Since the model and support system were symmetrical, the complete pressure distributions at angles of attack could be obtained with the same orifices by taking readings at both negative and positive angles of attack. The one-inch base had one base pressure orifice located at the center. The two-inch base contained six base pressure orifices, one at the center and the other five equally spaced around the lower right quadrant at a radius of 7/8 inch. The four-inch base was equipped to measure three base pressures at a radius of 1.2 inches and three base pressures at

Experimental Equipment (Cont'd)

a radius of 1.8 inches; the orifices in each ring were equally spaced at 45° increments in the lower left quadrant. The orifices on the four-inch base were formed by laying 1/16 inch copper tubing flat on the base and drilling 1/32 inch holes in the side of the tube at the aforementioned locations. One additional flush orifice was provided at the center of the four-inch base to be used when the sting was not present. Figures 2 and 3 show the orifice locations.

The wing span was 60 inches with a chord of 15.13 inches and a maximum thickness of 2 inches. The forward section of the wing was an aluminum extrusion, and the aft section was made from two pieces of rolled sheet-steel riveted together at the trailing edge.

The dummy stings, one inch and two inches in diameter respectively, and approximately 40 inches long, could be mounted in cantilever fashion from the base of the model. The one-inch sting was made of brass and could be used with all bases. A small pod or a short strut (shown in Fig. 4) could be mounted on the one-inch sting to vary the effective length of the sting. The two-inch sting was made of steel tubing and could be used with either the two inch, four inch or six inch base. Both stings, fitted with aluminum tail plugs faired to a point, were provided with orifices (shown in Fig. 3) to measure the pressure distribution along the sting.

III. Test Procedure

A. Tunnel Airflow Calibration

The tunnel airflow calibration was conducted with the main strut and the main image windshields installed at the trunnion spacing used in the test, without the model and tail struts, but with a calibrated pitot-static tube mounted on the tunnel axis at the center of the test section, measuring both the static and the dynamic pressure. The static-pressure gradient (see Fig. 6), measured along the tunnel axis, was obtained in a similar manner by mounting the pitot-static tube at various positions along the tunnel axis.

B. Angle of Attack Calibration

The angles of attack as presented herein are referred to the effective zero angle of attack. The effective zero angle of attack was defined as the angle at which the upper and lower pressure distributions over the fuselage were as nearly equal as possible. This was accomplished by connecting the top and bottom orifices at each fuselage station to adjacent manometer tubes and, with the tunnel at the dynamic pressure used in the test, adjusting the model angle of attack until the adjacent tube heights were as nearly equal as possible (i.e. it was not possible to get all pairs of tube heights equal simultaneously). This angle was 0.6° less than the angle at which the horizontal plane of symmetry of the model was level. The angle of attack indicator (shown in Fig. 1) was calibrated by the use of a precision bubble-protractor mounted on the wing of the model.

C. Operating Procedure

The operating procedure was to photograph each multiple manometer at every angle of attack. The angle was increased both positively and

Test Procedure (Cont'd)

and negatively from zero, allowing sufficient time at each angle for the manometers to come to equiblibrium before the pictures were taken. The model was carefully sealed after each configuration change to prevent any flow through the model and the seams faired to give a smooth surface. The wing tips were sealed with cellulose tape and the fuselage sides and base were sealed with tunnel wax. When the dummy strut was used, the angle of attack of the model could not be varied, because it was necessary to stabilize the dummy strut by guy-wires fastened to the tunnel walls. A few visual readings of the critical orifices were recorded to estimate the magnitudes of the sting effect, so that the short time available might be used to the best advantage. These data indicated that the sting-interference, for configurations where the base diameter to the sting diameter ratio was greater than two, would be extremely small. For this reason, it was decided not to run any of the tests on the six-inch diameter base, but to spend the available time in attempting to investigate more thoroughly the sting-interference effects with the smaller base diameters. Records were kept of body surface flaws and of orifice faults, in order to facilitate the checking of discrepancies in the data.

In addition to the photographic and visual data, micromanometer data for orifice A-17 (see Fig.2) were recorded. During the latter part of the investigation, micromanometer data were taken for configuration $B_1 + S_1$ at several orifices located at both fore and aft fuselage stations (see Section VI).

IV. Methods of Reduction and Presentation of Data

A. Reduction of Data

The photographic pressure data reduced and presented in this report are the data at $\alpha = 0^{\circ}$ for all configurations, and the data at $\alpha = 4^{\circ}$ for those configurations with B_2 which show the effects of varying the effective sting length by the pod. These photographically recorded data were reduced to static-pressure coefficients (defined on page 5) by projecting the recorded manometer image on a ground glass plate and measuring the fluid height in each tube relative to the manometer reference tubes used to indicate the tunnel dynamic pressure. The recorded micromanometer data were reduced but not presented in the report (see Section VI).

The data were not corrected for the static-pressure gradient along the axis of the test section (Fig. 6), because only the increments in the pressure coefficients, not the absolute magnitudes, were of interest in this investigation. It was not necessary to apply any blockage correction to the dynamic pressure, because the tunnel airflow was calibrated at the dynamic pressure of the test with the main strut and main image-windshields installed, and the volume of the model was sufficiently small that the blockage at this low Mach number could be neglected.

B. Presentation of Data

All data are presented in the form of plotted points and faired figures. All plotted points represent experimental observations and are faired as consistently as possible with consideration of the faulty orifices.

The pressure distributions over the surfaces of the body and the sting are plotted as $\frac{p}{q}$ vs. x (where "x" is the axial distance of the orifice in inches downstream from the nose of the model) for

Methods of Reduction and Presentation of Data (Cont'd)

various values of the polar angle θ (see Figures 2 and 3). Plots were made covering the entire length of the fuselage for configurations B, B_1, B_2 and B_4, at $\alpha = 0^o$, to show the basic pressure distribution over the body and the effects of cutting off the tail. For all other axial pressure distribution plots, the data are plotted only for the aft section of the fuselage and the forward section of the sting. These plots show the effects of varying the ratio of the base diameter to the sting diameter, and the effects of varying the effective sting length.

The base pressure data (see Fig. 3 for the orifice locations) are presented in plotted form in three ways. For the configurations with the two-inch diameter base, the data are plotted as $\frac{p}{q}$ vs. polar angle θ, and as $\frac{p}{q}$ vs. y, the effective sting length in inches. For configurations with the four-inch diameter base, the data are plotted as $\frac{p}{q}$ vs. r, where "r" is the radius of an orifice ring, in inches , measured on the base.

V. Experimental Results and Discussion

Before discussing the results, it is of interest to examine the data to obtain some idea of the basic accuracy and principal sources of error. The test dynamic pressure of 60 psf (corresponding Reynolds number based on the maximum body diameter equal to 8.5×10^5) was held constant within 0.1 percent. From the standpoint of accuracy of the multiple manometer data, a higher dynamic pressure was desirable, but the tunnel power limited it to 60 psf. Even at this low speed the readings of the pressure from the manometer film could, with care, be repeated to within 0.003 in $\frac{p}{q}$. The error in $\frac{p}{q}$ for a single tube, however, could possibly be as large as 0.01 (corresponding to a change of 3.6 mm in fluid height on the manometer) due to fluctuations in the fluid heights. At the low angles of attack, fluctuations in the fluid heights were of the order of 2 to 3 mm.

There was about 0.3 degree play in the joint between the model and the pitch drive mechanism. The model, however, did not appear to vibrate in the tunnel, thus this play was considered to have introduced very little error.

The condition of an orifice had a great deal to do with the pressure reading obtained. Both during and after the test, checks were made to locate the faulty orifices. Some of the orifices were loose and protruded, and others gave obviously erroneous readings due to leakage, or by being plugged. These facts were considered in fairing the data to obtain more representative pressure distribution curves.

The basic pressure distribution over the entire body length, as shown by Figures 7 to 9, compares favorably with the theoretical pressure distribution over similar bodies (see Ref. 1). These data also show that the basic pressure distribution over the body is not altered, within the accuracy of these experiments, by cutting off the tail of the fuselage,

Experimental Results and Discussion (Cont'd)

except perhaps very near to the tail of the body. The data for configuration B at the polar angle of zero degrees (Fig. 7) appear to fall consistently above the average curve for the other bodies. However, this trend is not borne out by the data at the two other polar angles (Figures 8 and 9) and hence is not felt significant, in view of the fact that the basic accuracy of the data is 0.01 in $\frac{p}{q}$. The data for orifices aft of the wing show a degree of scatter at $\theta = 90^{\circ}$ (Fig. 9) which is probably caused by the wake of the wing, which covers these orifices. The data at $\theta = 90^{\circ}$ for orifices forward of the wing indicate that the nose is probably yawed slightly to the left.

Figures 10 to 18 show more clearly the effects on the aft portion of the fuselage caused by cutting off the tail. Configuration B_1 indicates a decrease in pressure, but in light of the foregoing discussion, the results are inconclusive. There appears to be no measurable effect when the body is cut off at the two-inch base. There is a small but measurable increase in pressure shown by the data for configuration B_4. This evidence is insufficient to show any definite effects.

The effects of the ratio of the base diameter to sting diameter are shown on these same figures. The sting length is these figures is considered to be infinite (i.e. the sting extended into the tunnel diffuser section and was faired to a pointed end.) These data show that the presence of the sting increases the pressure over the aft portion of the body, and that this effect increases as the sting diameter approaches the base diameter. When the ratio is one, this effect becomes larger and extends further forward on the fuselage as the base diameter is increased.

The effects of varying the effective sting length, when the base diameter is one inch and the base diameter to sting diameter ratio is one, are shown in Figures 19 to 24. The pressure over the aft portion

Experimental Results and Discussion (Cont'd)

of the fuselage increases as the effective sting length is shortened. However, the magnitude of the increase, on the periphery of the base, caused by shortening the sting length to four inches with the pod (diameter of four inches and finess ratio of 3), is approximately one-half the increase caused by the presence of the effectively infinite sting. This "short-sting" pressure-increase has, within the accuracy of these measurements, dropped to zero 6 inches forward of the base. When the dummy strut (12 inch chord, 2 inch maximum thickness, and 39 inch length) is used to shorten the effective sting length to six inches, the pressure increase on the periphery of the base is very nearly the same as the increase caused by the pod at four inches, but extends ten inches forward from the base. When the dummy strut is used to vary the sting length, there is a slightly larger pressure increase at $\theta = 0^{\circ}$ than at $\theta = 180^{\circ}$. This is to be expected as the dummy strut is not symmetrical with respect to the horizontal plane but extends 36 inches below it and only 3 inches above it. This effect is substantiated by the pressure indications from orifices at $\theta = 0^{\circ}$ and $\theta = 180^{\circ}$ on the sting, in the region just forward of the strut. However, this asymmetry in the pressure distribution appears to die out quite rapidly upstream from the strut.

The effects of varying the effective sting length, when the base diameter is two inches and the base diameter to sting diameter ratio is two, are shown in Figures 25 to 30. The increase in pressure on the periphery of the base caused by shortening the effective sting length is greater than it was when the base diameter to sting diameter ratio was one. The magnitude of the increase caused by shortening the effective sting length to four inches with the pod is approximately three times the increase due to the introduction of the infinite sting. When the dummy strut is used, and the effective sting length is six inches, the

Experimental Results and Discussion (Cont'd)

"short-sting" pressure-increase is more nearly twice the increase caused by the presence of the effectively infinite sting. For both the pod and the strut, the "short-sting" pressure increase appears to drop to zero eight inches forward from the base. Figure 28 substantiates the asymmetrical pressure-increase (shown in Fig. 22) caused by the presence of the dummy strut but indicates no asymmetry on the periphery of the base even at the shortest effective sting length.

Figures 31 to 35 show the effects of varying the effective sting length with the pod, when the base diameter is two inches and the base diameter to sting diameter ratio is two, at $\alpha = 4^{\circ}$. While these data show no appreciable change from the data at $\alpha = 0^{\circ}$, they do constitute seperate readings that help to establish the repeatability of the data.

The effects of the presence of the sting on the base pressure at $\alpha = 0^{\circ}$ and $\alpha = 4^{\circ}$, when the base diameter is two inches and the ratio of the base diameter to sting diameter is two, are shown in Figures 36 and 37. Figure 36 indicates that the pressure is constant over the base at $\alpha = 0^{\circ}$, and the introduction of the sting has little effect. However, Figure 37 indicates a slight decrease in the average base pressure when the angle is changed to four degrees and also a slight increase in base pressure, at the measuring radius, as θ increases from 0° to 180°: The effect of the presence of the sting, at $\alpha = 4^{\circ}$, is to increase the pressure over the base to a constant value, slightly higher than that shown at $\alpha = 0^{\circ}$, with the sting present. The effect of the two-inch sting on the four-inch base (Fig. 38) indicates no effect caused by the presence of the sting except at $\theta = 90^{\circ}$. It is possible that the values at 90° are influenced by the wing wake, although no effect of wing wake is apparent in the data for the two-inch base.

Figures 39 and 40 show the effects of decreasing the effective sting length at $\alpha = 0^{\circ}$ and $\alpha = 4^{\circ}$. The base pressure approaches the

Experimental Results and Discussion (Cont'd)

value for the infinite sting more rapidly for the pod than it does for the dummy strut. No variation, in the base pressure over the base, caused by the asymmetry of the dummy strut was observed.

VI. Conclusions

The evidence gathered from the tests indicates several trends. When the ratio of the base diameter to the sting diameter is two, the presence of the effectively infinite sting produces an increase in pressure over the aft portion of the body at zero angle of attack. This pressure increase is of the order of one percent of the dynamic pressure at the rear edge of the body, but has dropped to zero at a distance of three sting diameters forward of the base. There is no definite effect on the base pressure, caused by a sting whose diameter is half of the diameter of the base, at zero angle of attack. However at four degrees angle of attack, the presence of the sting increases the base pressure approximately one percent of the dynamic pressure. When the ratio of the base diameter to the sting diameter is one, the presence of the effectively infinite sting produces an increase of approximately five percent of the dynamic pressure on the periphery of the base; this increase drops to zero four sting diameters forward of the base.

The effective sting length becomes infinite when the actual sting length is equal to four times the diameter of the sting supporting structure, if this structure is a three dimensional body. If the sting is supported by a straight strut, then the effective sting length becomes infinite when the actual sting length is equal to one and one-half times the strut chord. This effect is shown by both the peripheral and base pressures when the sting diameter is one-half the base diameter, and by the peripheral pressures when the sting diameter equals the base diameter.

This investigation indicates that if more data are desired at this low dynamic pressure, a more accurate method of measuring the model pressures is needed, as the sting effects are of the same order of

Conclusions (Cont'd)

magnitude as the accuracy of the pressure data. During the last part of the test an attempt was made to measure the model pressures more accurately with a micromanometer. However, the fluctuations in the fluid height were of a magnitude such that, to obtain a representative reading of sufficient accuracy, the manometer had to be observed over a period of approximately three minutes and the average value recorded. These fluctuations were observed for orifices both on the fore and aft portions of the fuselage. A one gallon plenum was installed in the pressure line leading to the orifice in an attempt to damp out these fluctuations, but it was not effective. Insufficient tunnel time was available to allow further investigation of these fluctuations and their causes.

Inclined multiple manometers might be used to increase the relative fluid heights and thereby reduce the percentage error. A better method, however, would be to run the tests at a higher dynamic pressure.

References

1. Brand, M., "Druckverteilungen Von Rotationskorpern Bei Achsialer Anstromung," Aerodynamische Versuchsanstalt Gottingen e. V. UM Nr. 3206, December 30, 1944.
2. Hemke, Paul E., "Influence of the Orifice on Measured Pressures", NACA TN 250, November,1926.
3. Delano, James B., "Pressure Distribution on the Fuselage of a Midwing Airplane Model at High Speeds," NACA TN 890, February, 1943.
4. Corson, Blake W. Jr., "The Belt Method for Measuring Pressure Distribution," NACA WARTIME REPORT L-244.
5. Freeman, Hugh B., "Pressure-Distribution Measurements on the Hull and Fins of a 1/40-Scale Model of the U. S. Airship "AKRON", NACA TR 443, 1932.

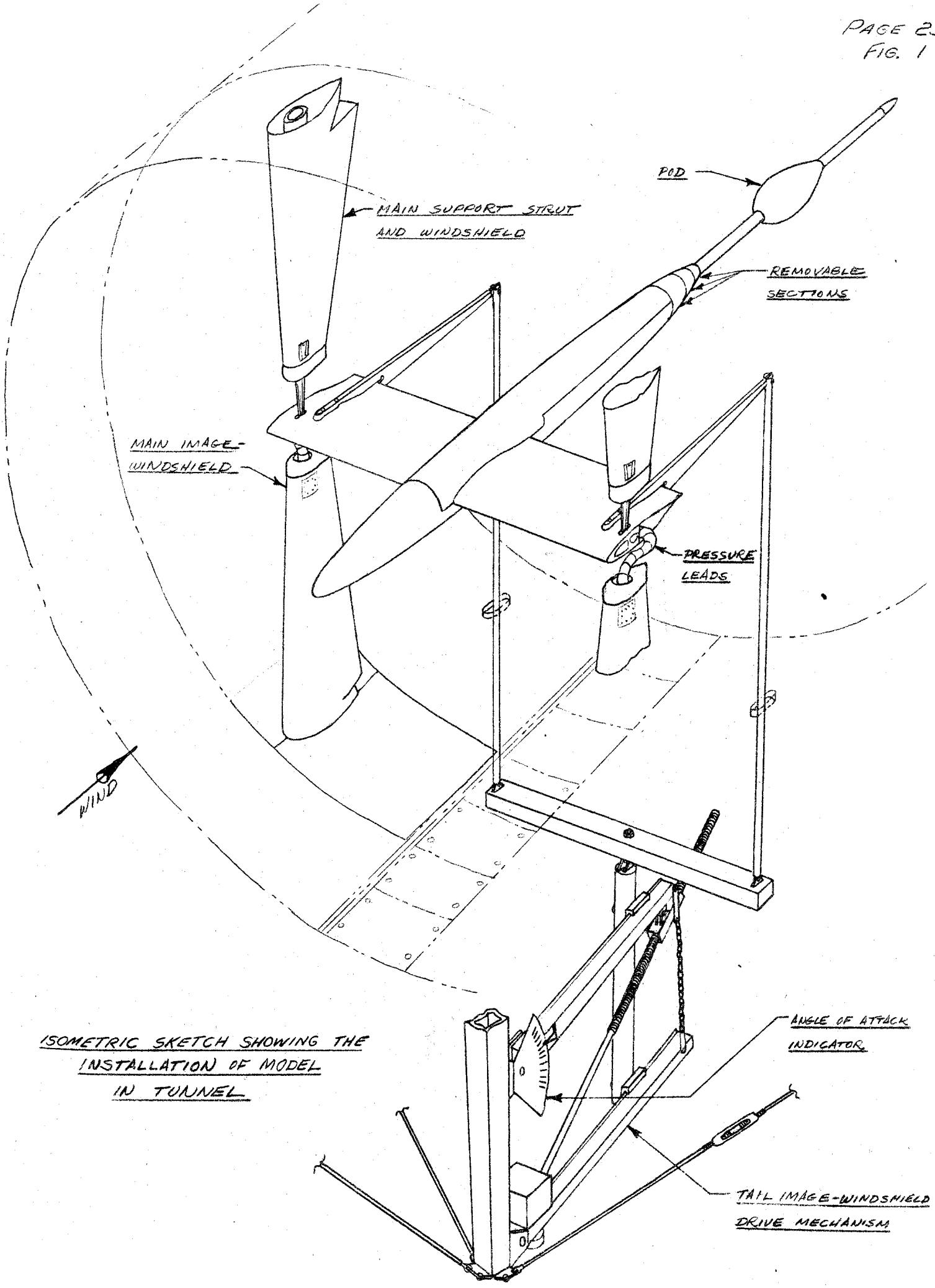

ISOMETRIC SKETCH SHOWING THE INSTALLATION OF MODEL IN TUNNEL

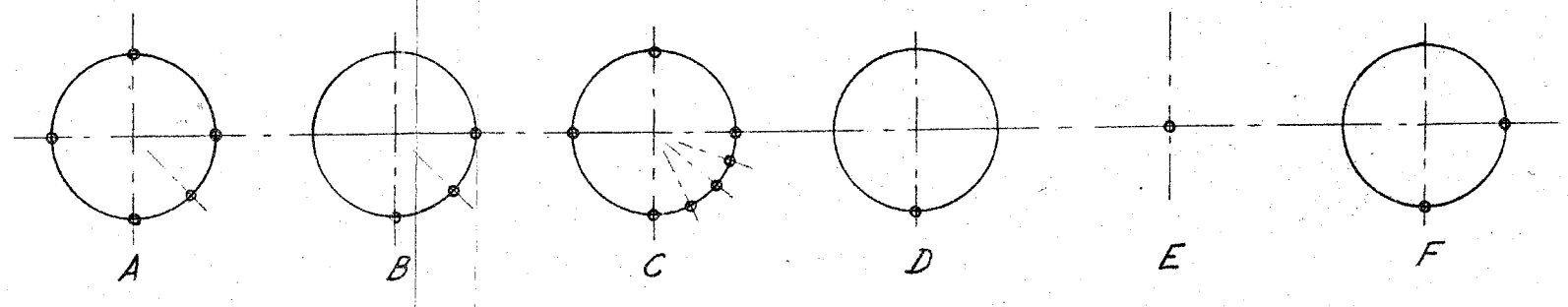

PRESSURE ORIFICE RING PATTERNS ~ LOOKING AFT

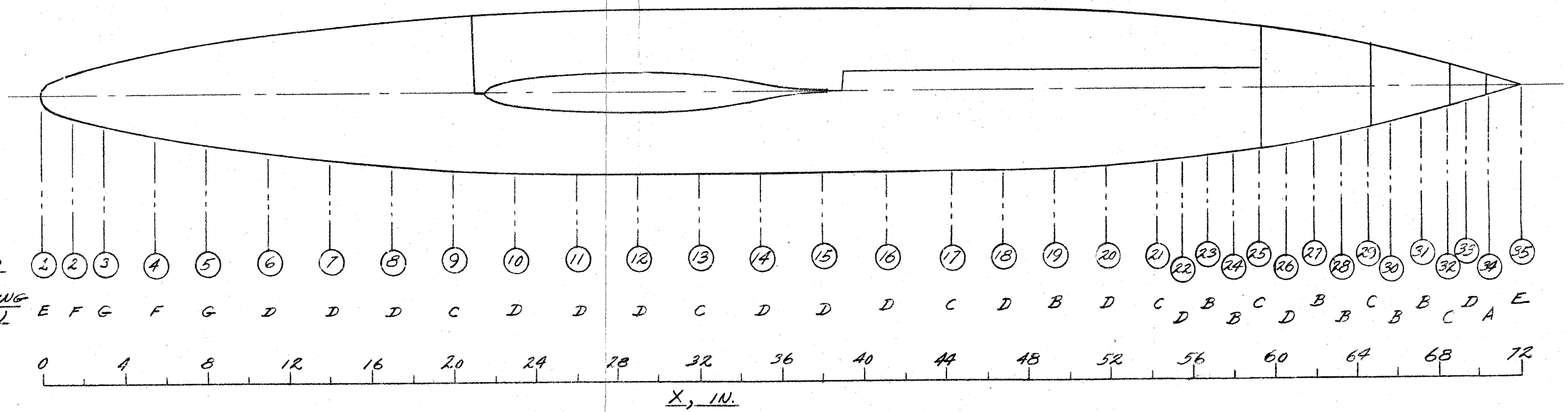

SKETCH SHOWING LOCATIONS OF ORIFICES ON THE BODY B

SCALE : 1 CM = 2 IN.

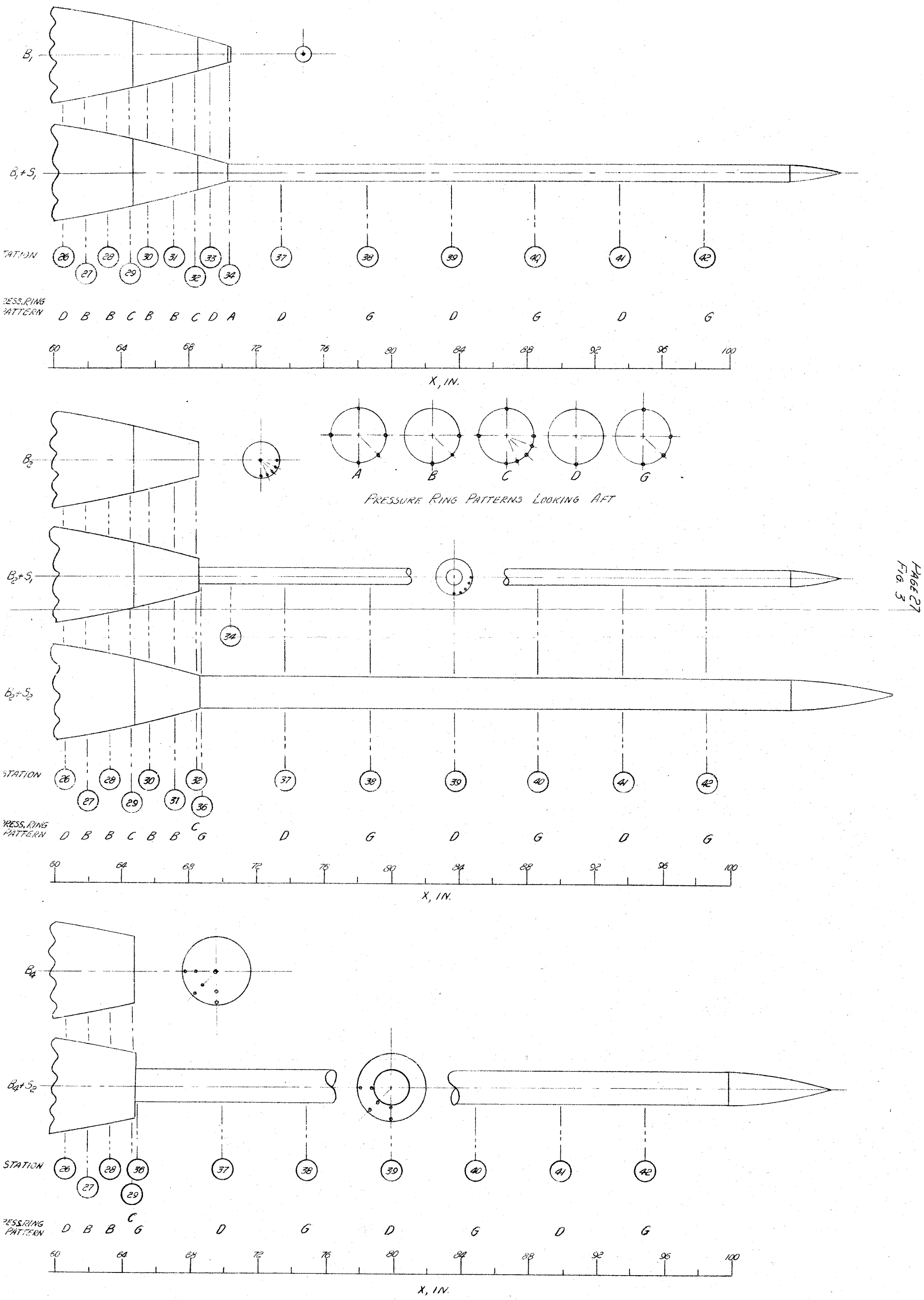

SKETCH SHOWING LOCATIONS OF THE BASE PRESSURE AND STING ORIFICES

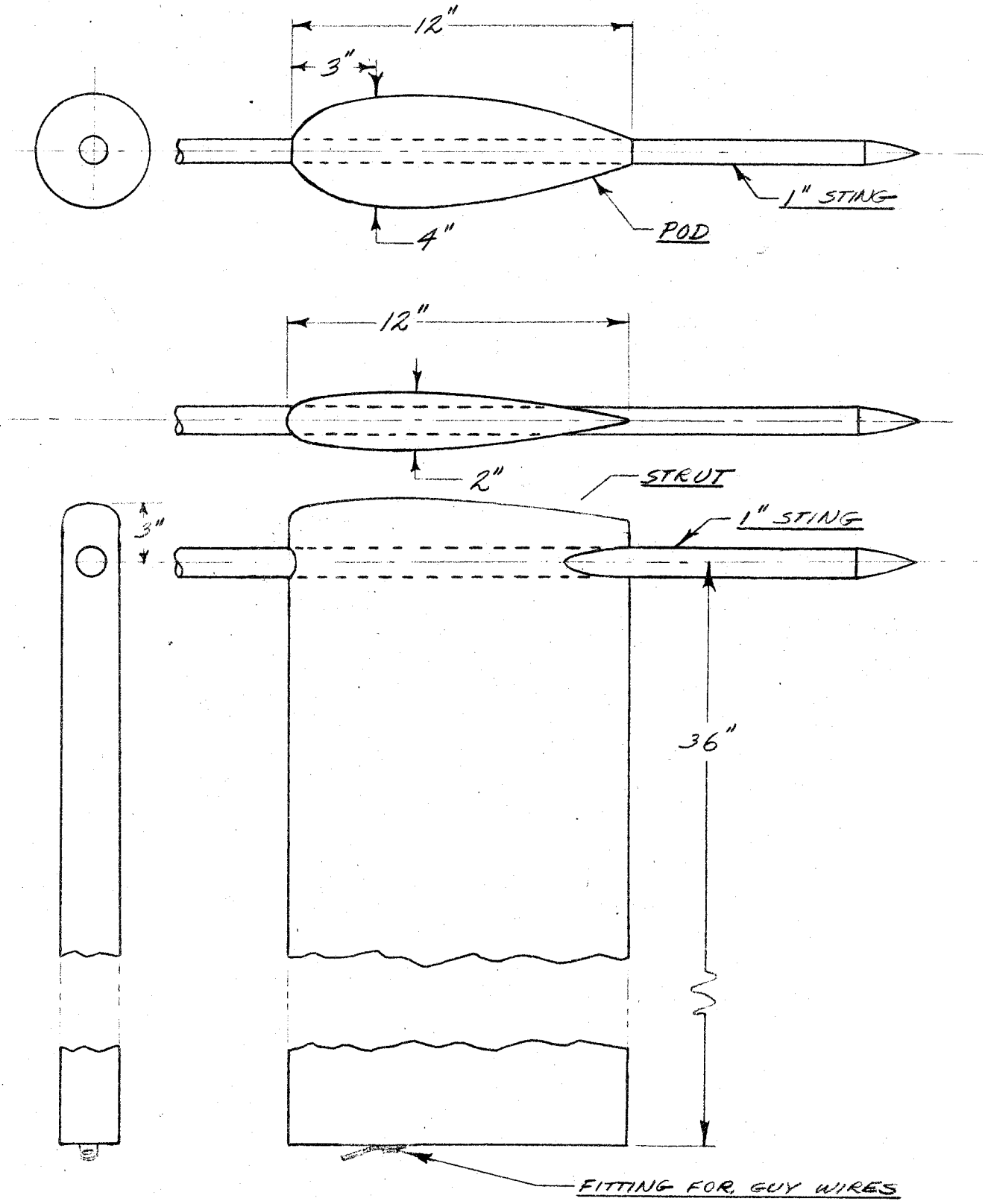

SKETCH OF POD AND DUMMY STRUT USED TO VARY THE EFFECTIVE LENGTH OF THE ONE-INCH STING

VERTICAL SECTION THROUGH 10 FT. WIND TUNNEL
2 PARAMETER 6 COMPONENT SUSPENSION SYSTEM
GUGGENHEIM AERONAUTICS LABORATORY
CALIFORNIA INSTITUTE OF TECHNOLOGY

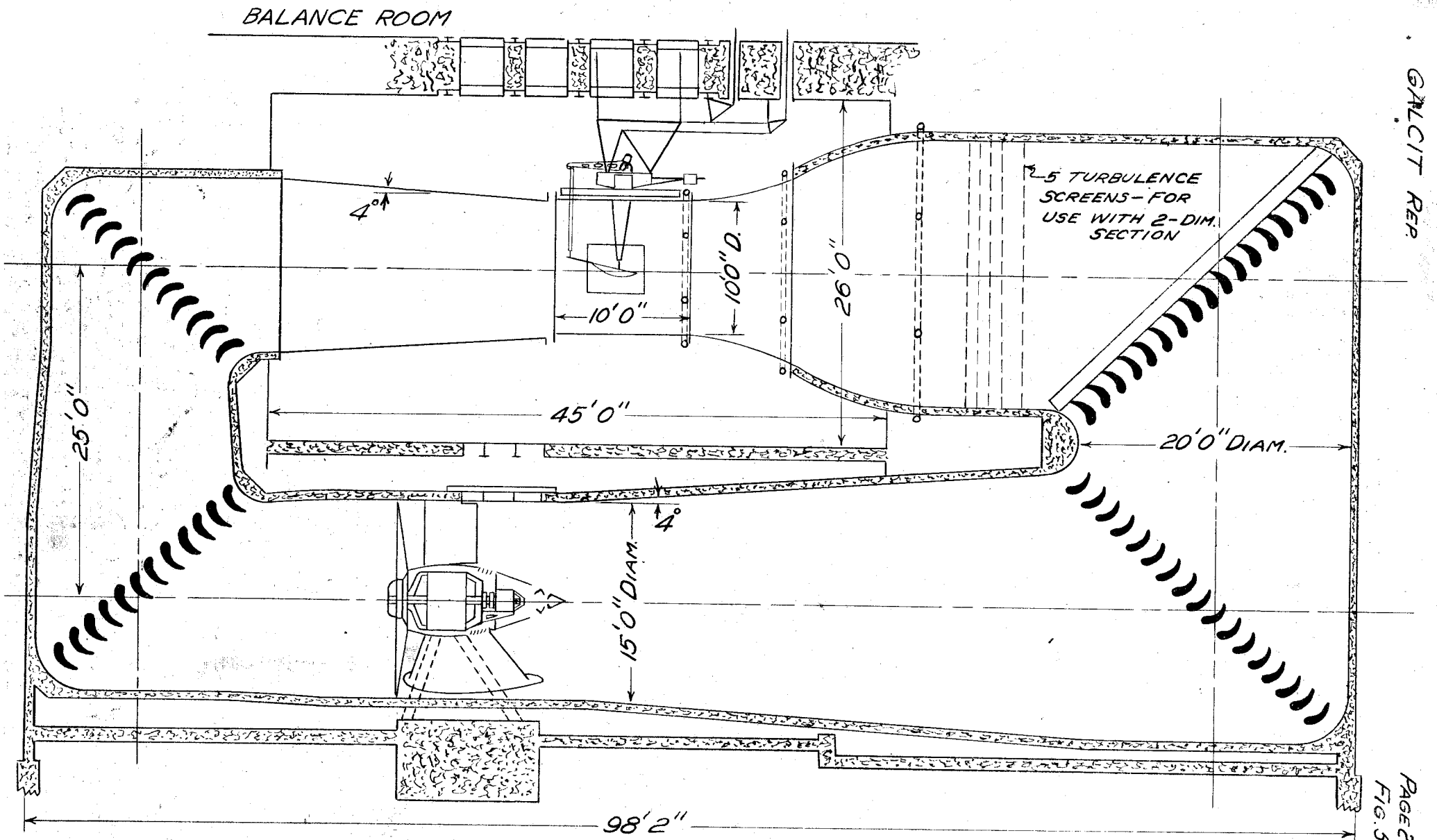

GALCIT REP.

PAGE 29
FIG. 5

STATIC PRESSURE SURVEY ALONG AXIS OF 10-FT. TUNNEL

$q = 60 \text{ LBS/FT}^2$
$\alpha = 0°, \theta = 0°$

○ B, RUN 3
△ B_1, " 9
□ B_2, " 4
▽ B_4, " 7

TAGGED SYMBOLS ARE $\theta = 180°$

LEADING EDGE OF WING

TRAILING EDGE OF WING

$\frac{F}{q}$ vs. x

EFFECTS ON COMPLETE BODY OF CUTTING OFF THE TAIL, $\alpha = 0°, \theta = 0°$

EFFECTS ON COMPLETE BODY OF CUTTING OFF THE TAIL, $\alpha = 0°$, $\theta = 45°$

$\frac{F}{q}$ vs α

$q = 60 \text{ LBS/FT}^2$
$\alpha = 0°$, $\theta = 45°$

○	B_0	RUN 3
△	B_1	" 9
□	B_2	" 4
▽	B_4	" 7

LEADING EDGE OF WING

LEADING EDGE OF WING

$\frac{F}{q}$

α

0 4 8 16 20 24 28 32 36 40 44 48 52 56 60 64 68 72

.04 .08 .12 .16 .20

$q = 60 \text{ LB/FT}^2$
$\alpha = 0°, \theta = 90°$

○ B, RUN 3
△ B_1, " 9
□ B_2, " 4
▽ B_3, " 7

TAGGED SYMBOLS ARE $\theta = 270°$

LEADING EDGE OF WING

TRAILING EDGE OF WING

.20
.16
.08
.04
0
.04
.08
.12

$\frac{p}{q}$

0 4 8 12 16 20 24 28 32 36 40 44 48 52 56 60 64 68 72

x

EFFECTS ON COMPLETE BODY OF CUTTING OFF THE TAIL, $\alpha = 0°, \theta = 90°$

$\frac{p}{q}$ VS x

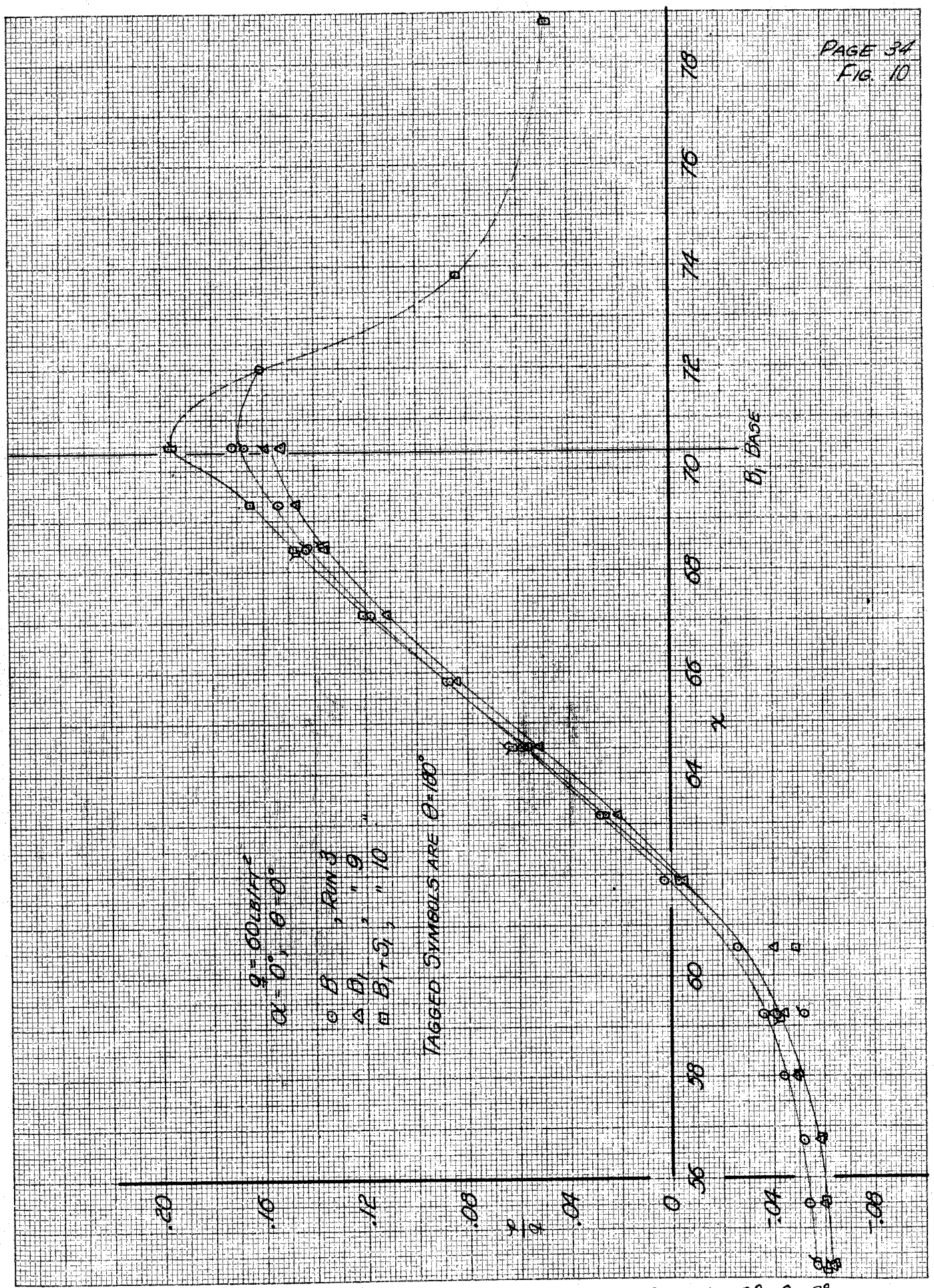

EFFECTS OF ONE-INCH STING ON B_1, $\alpha = 0°$, $\theta = 0°$

p VS X

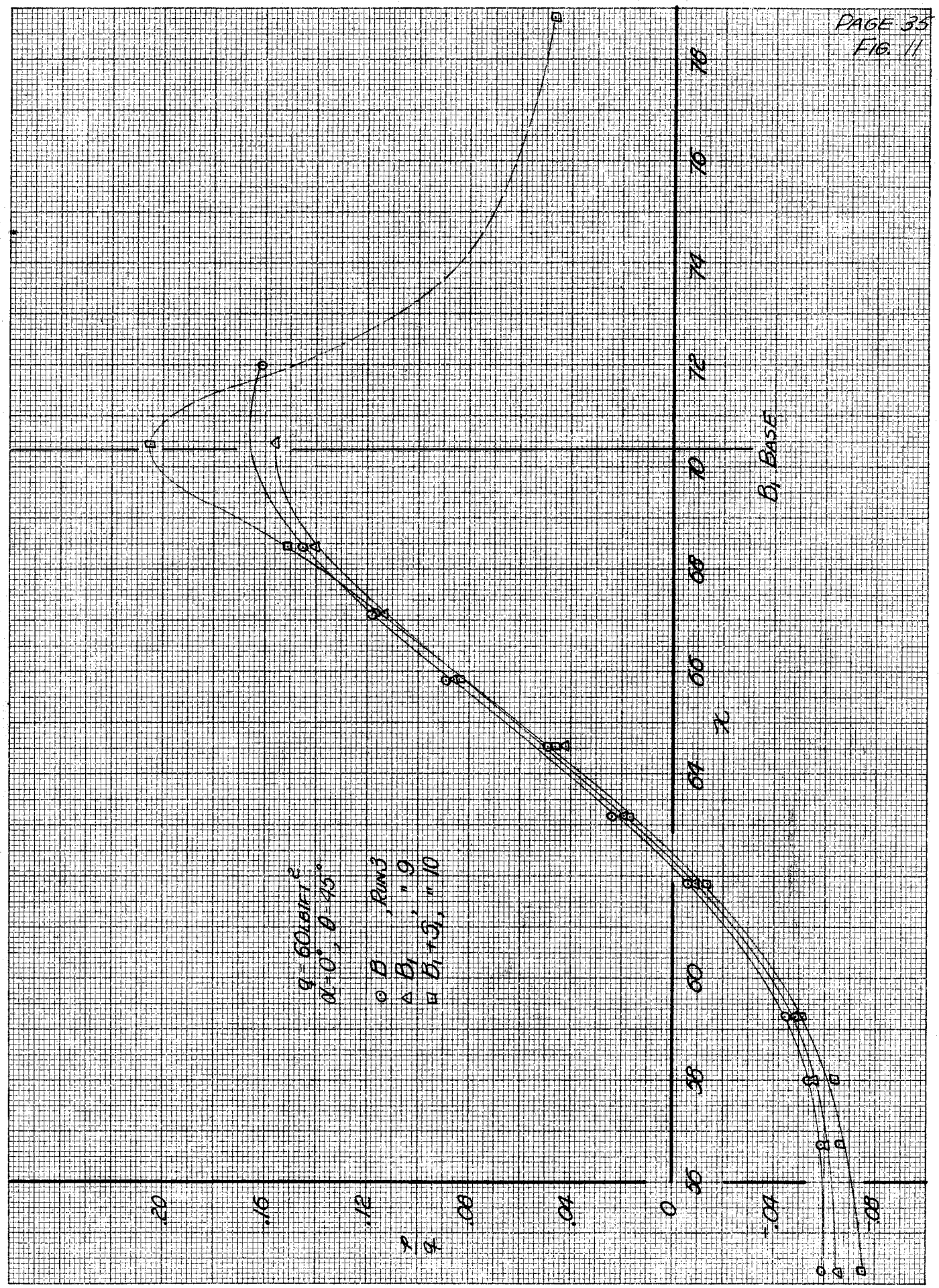

EFFECTS OF ONE-INCH STING ON B_1, $\alpha = 0°$, $\theta = 45°$

$\frac{z}{c}$ vs. x

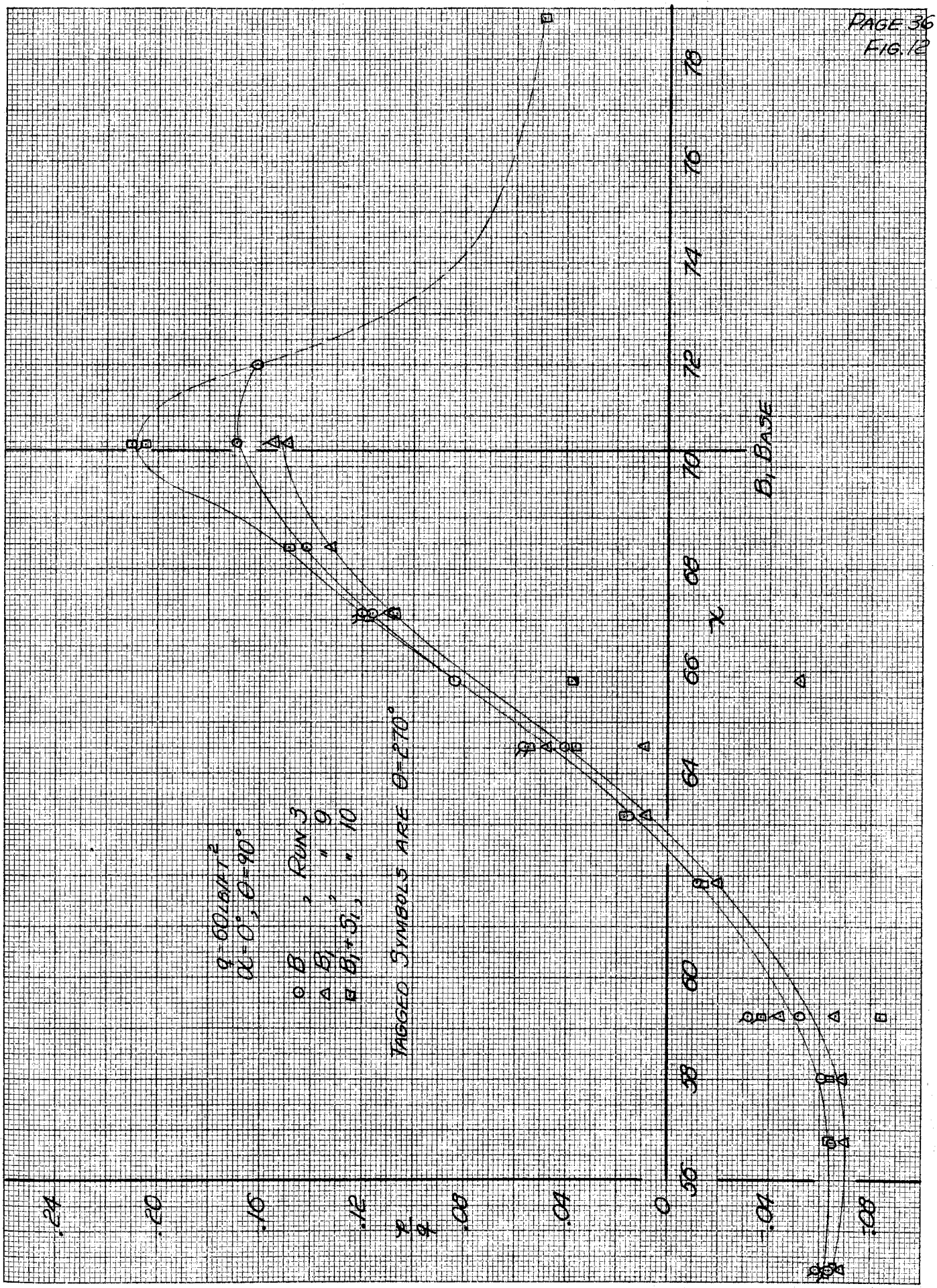

EFFECTS OF ONE-INCH STING ON B_1, $\alpha = 0°$; $\theta = 90°$

P VS. x

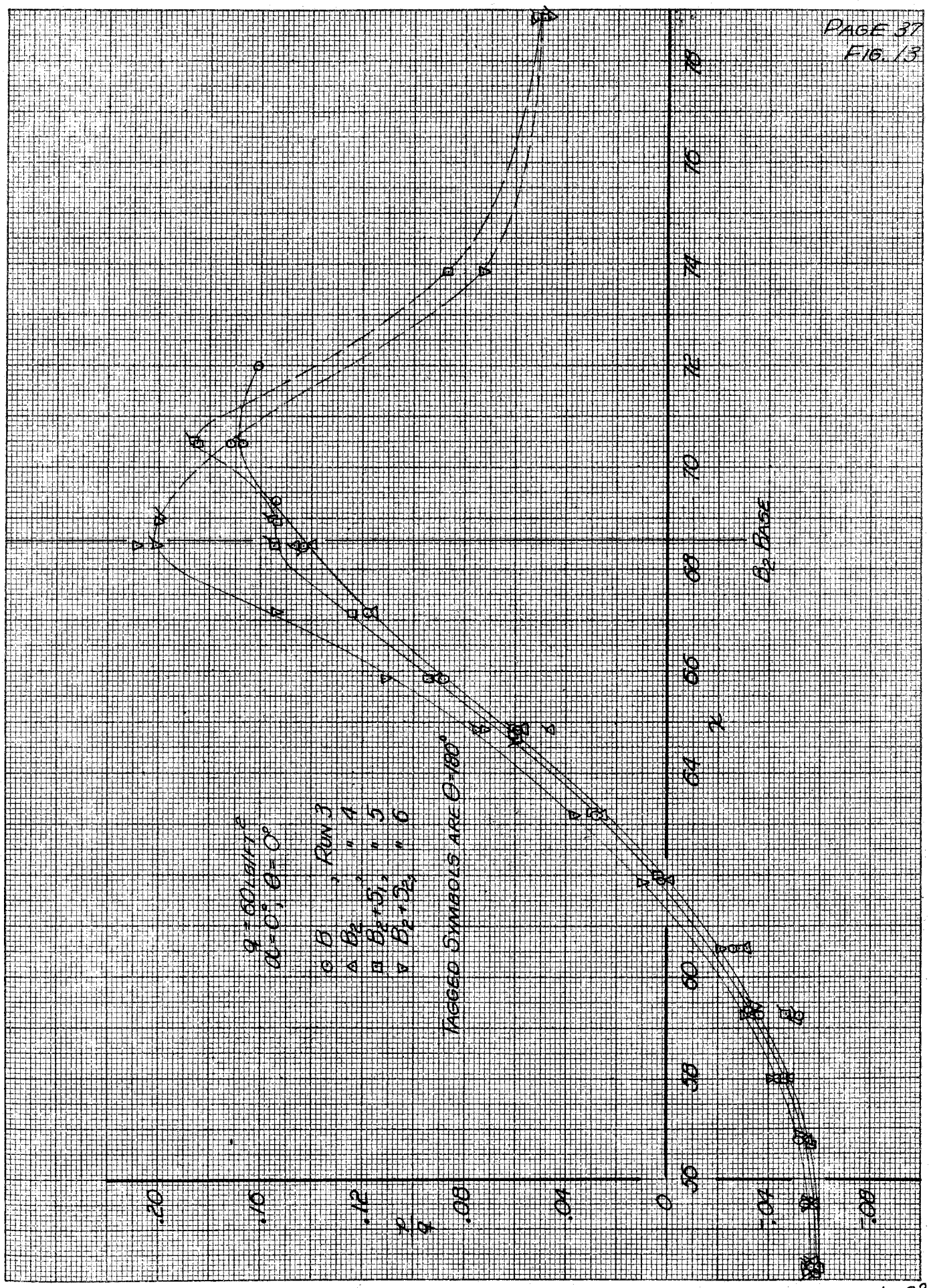

EFFECTS OF ONE-INCH AND TWO-INCH STINGS ON B_2, $\alpha = 0°, \theta = 0°$
$\frac{P}{P_0}$ VS. x

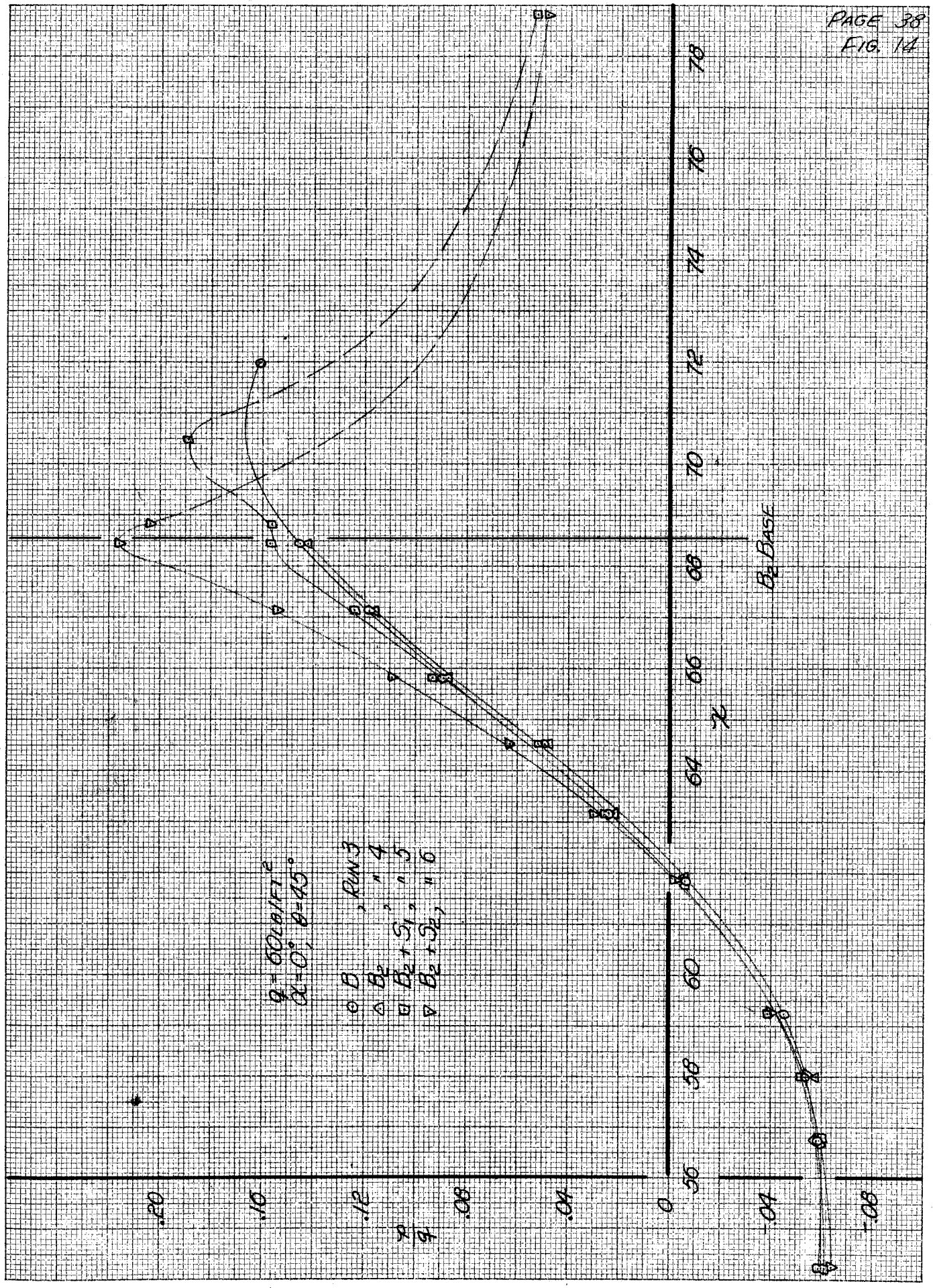

EFFECTS OF THE ONE-INCH AND TWO-INCH STINGS ON B_2, $\alpha = 0°$, $\theta = 45°$

L vs. w

FIG. 15

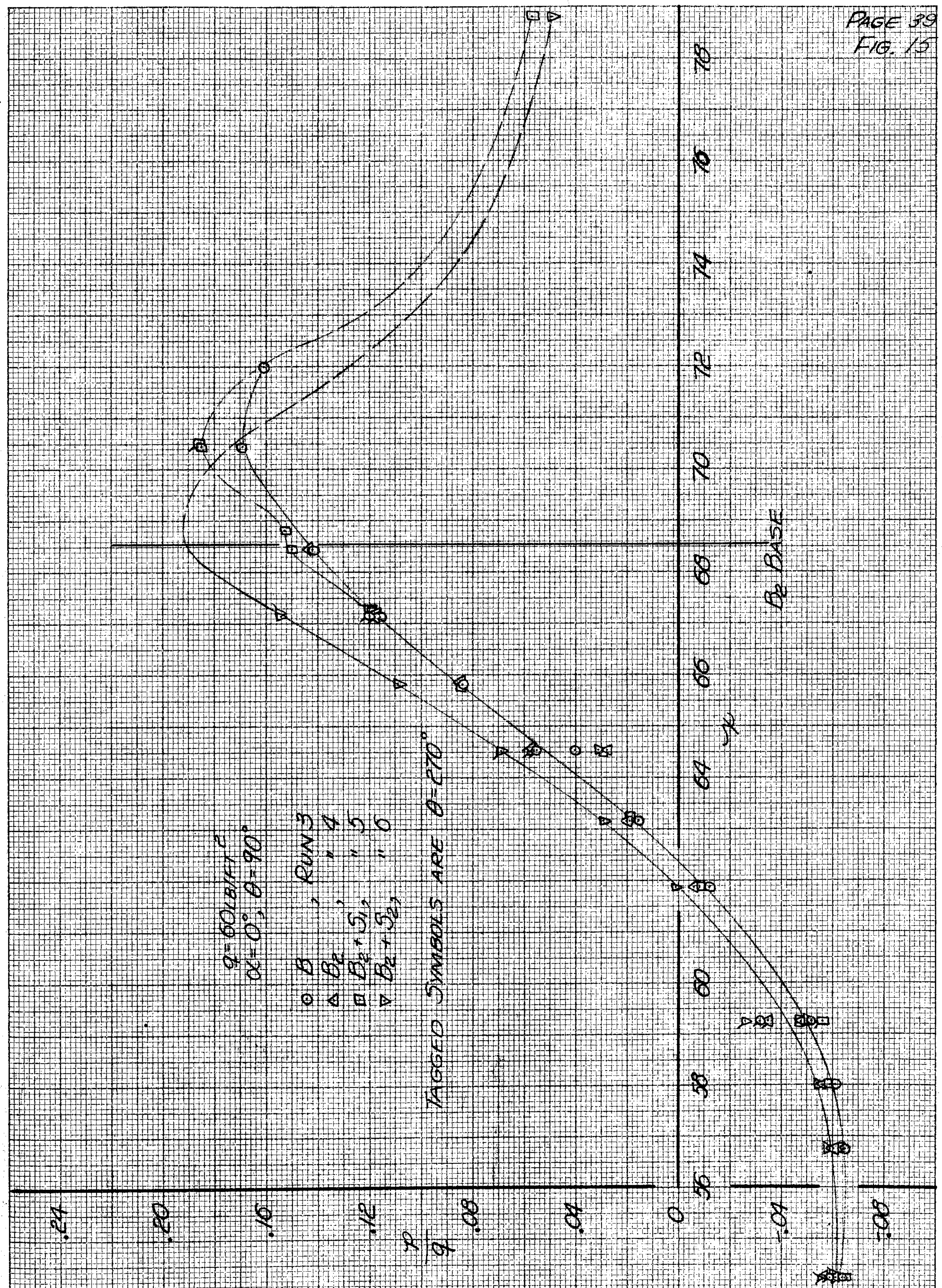

EFFECTS OF THE ONE-INCH AND TWO-INCH STINGS ON B_2, $\alpha = 0°$, $\theta = 90°$

$\frac{P}{q}$ VS. x

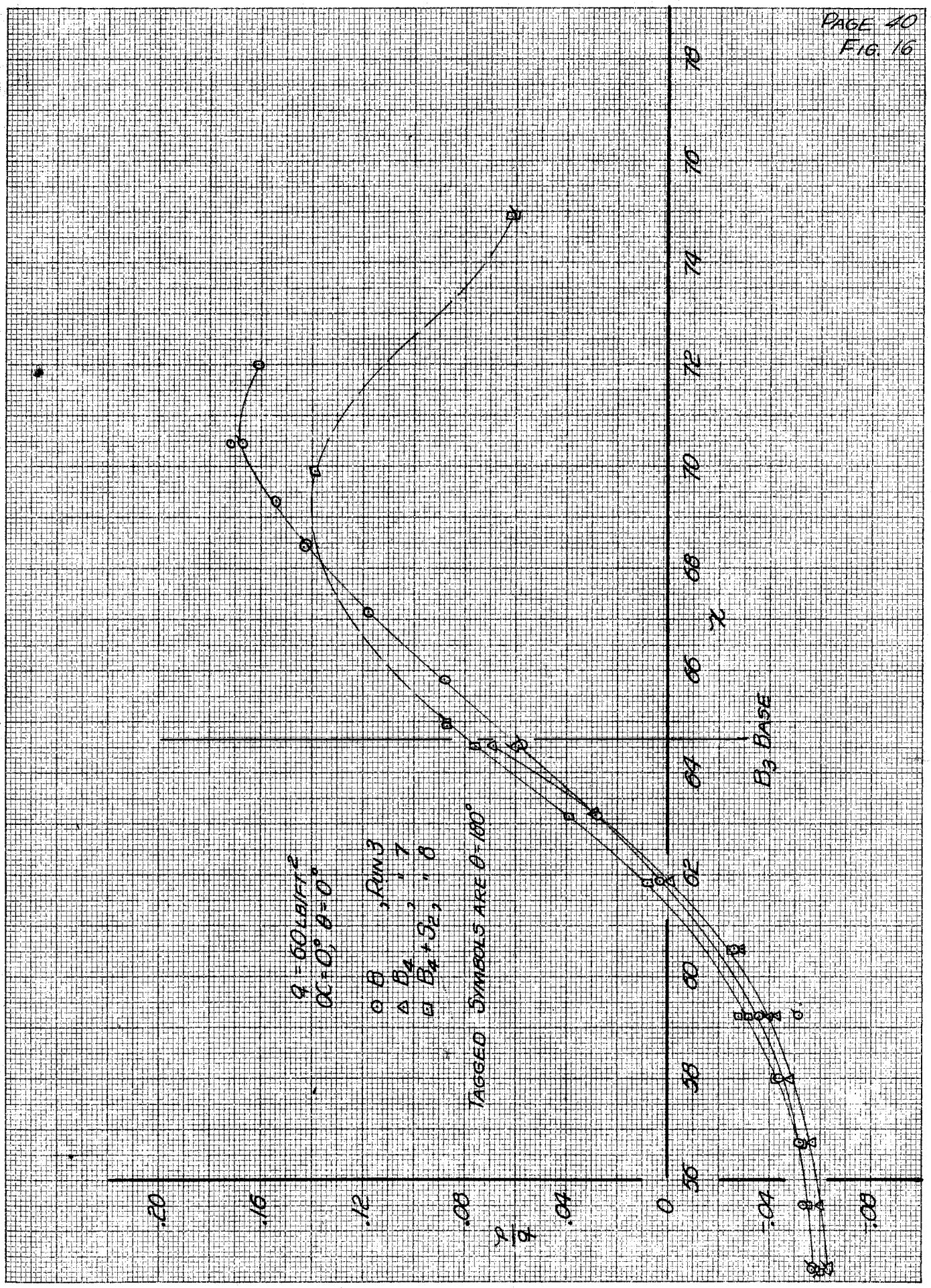

EFFECTS OF TWO-INCH STING ON B_4, $\alpha = 0°$, $\theta = 0°$

$\frac{p}{q}$ VS. x

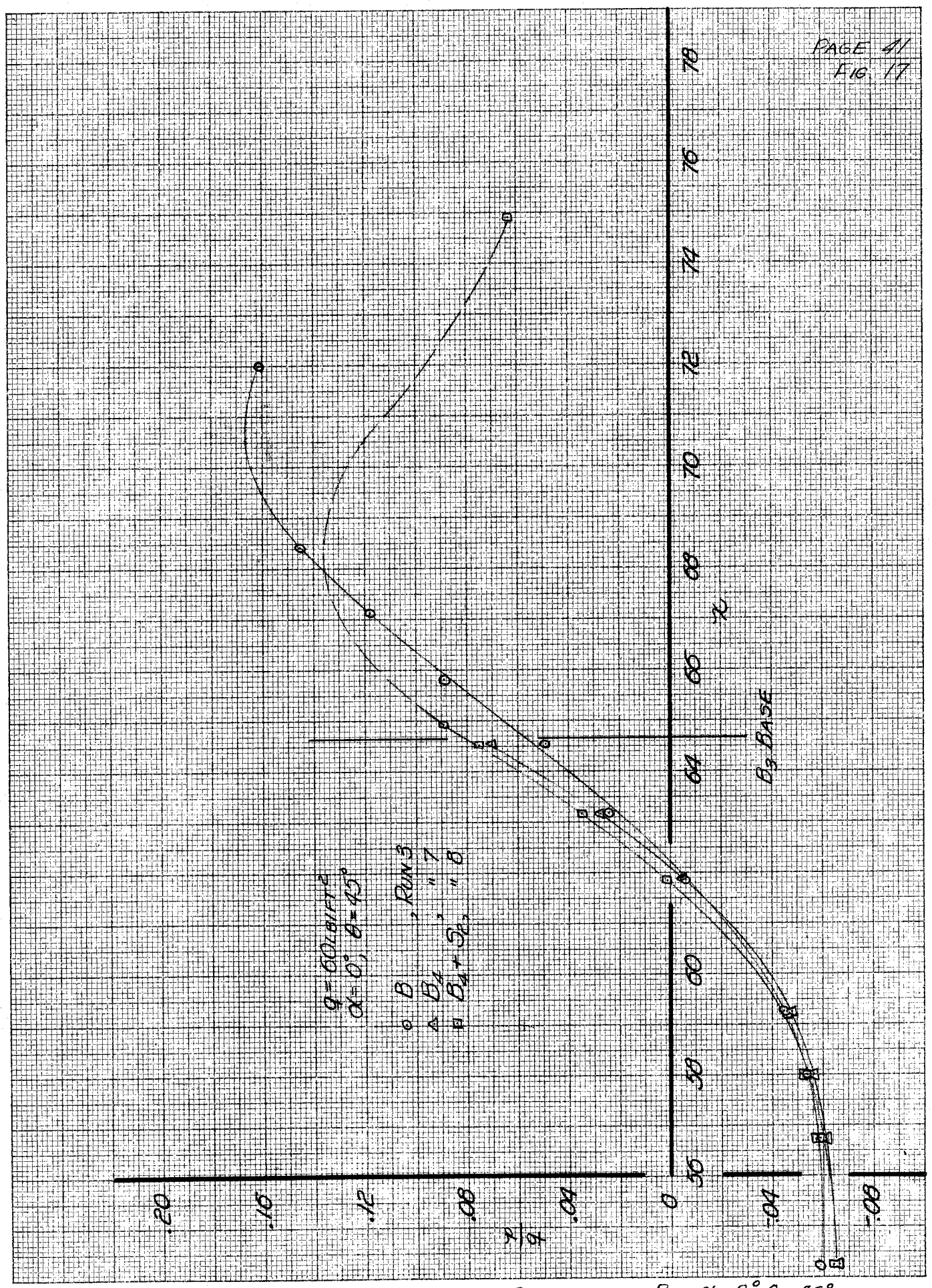

EFFECTS OF TWO-INCH STING ON B_4, $\alpha = 0°, \theta = 45°$

$\frac{P}{q}$ VS. $\frac{x}{t}$

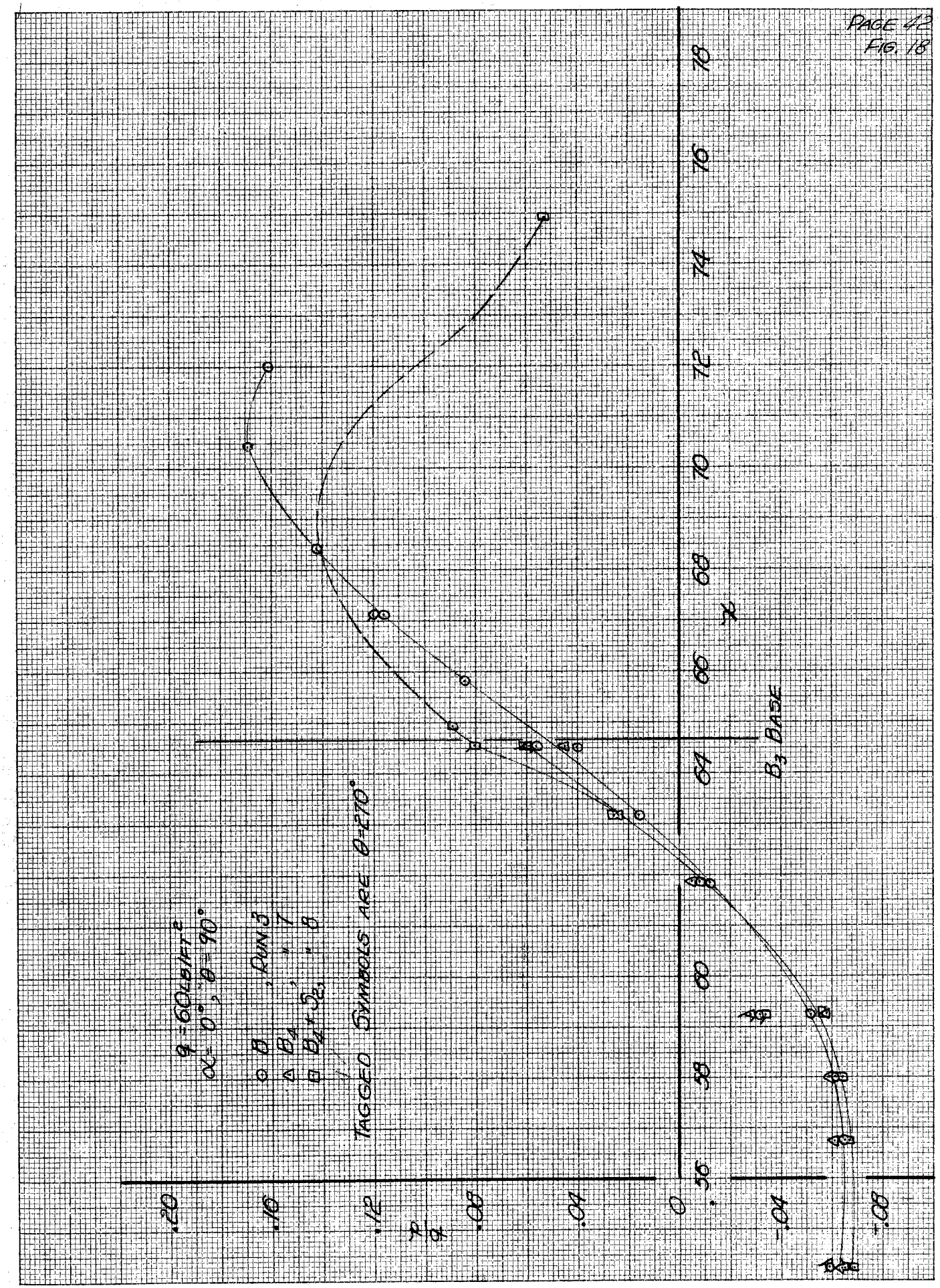

EFFECTS OF TWO-INCH STING ON B_4, $\alpha = 0°$, $\theta = 90°$

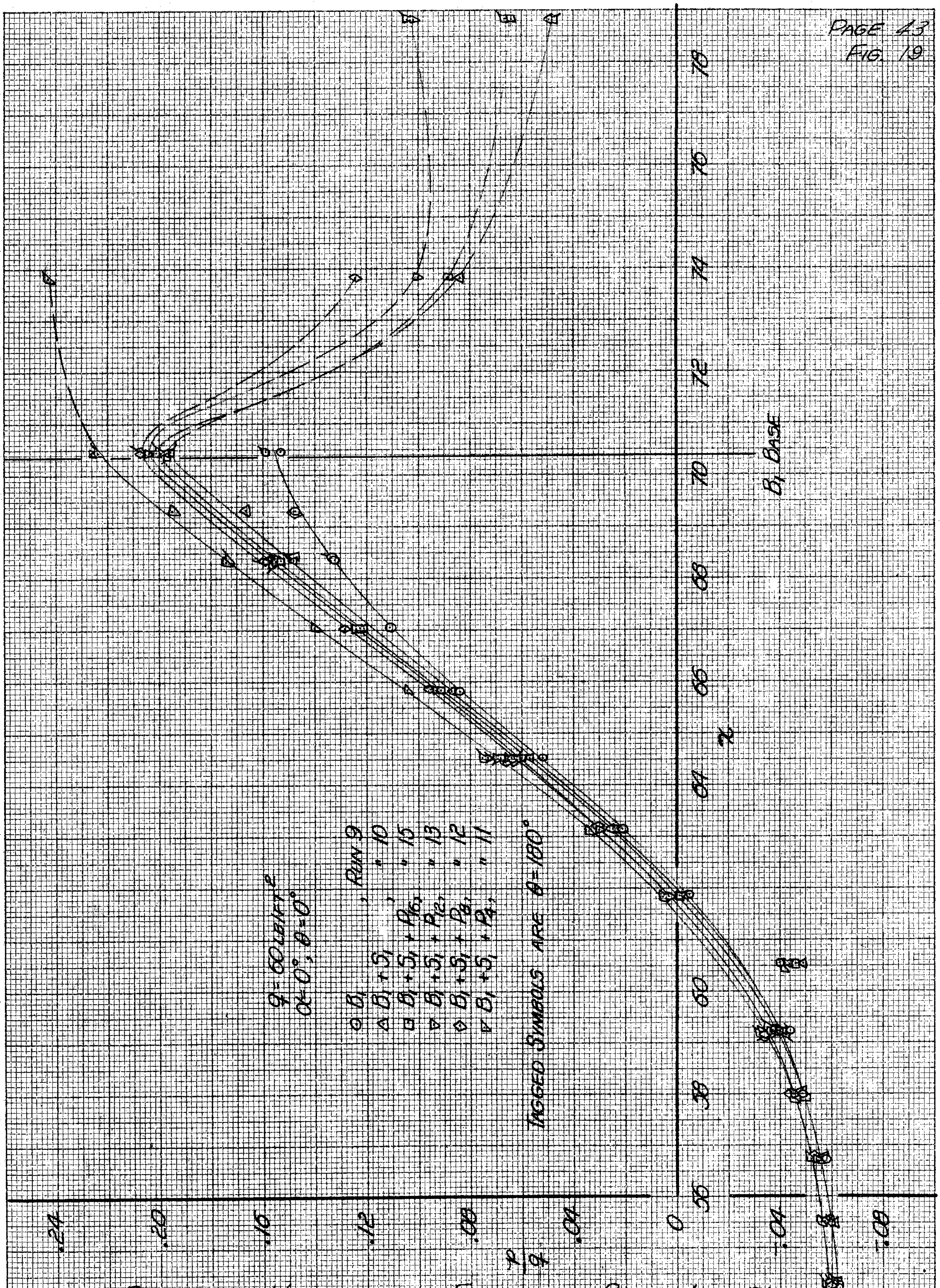

EFFECTS OF VARYING THE EFFECTIVE STING LENGTH

BY THE POD, CONFIGURATION B_1, $\alpha = 0^\circ$, $\theta = 0^\circ$

P/q vs x

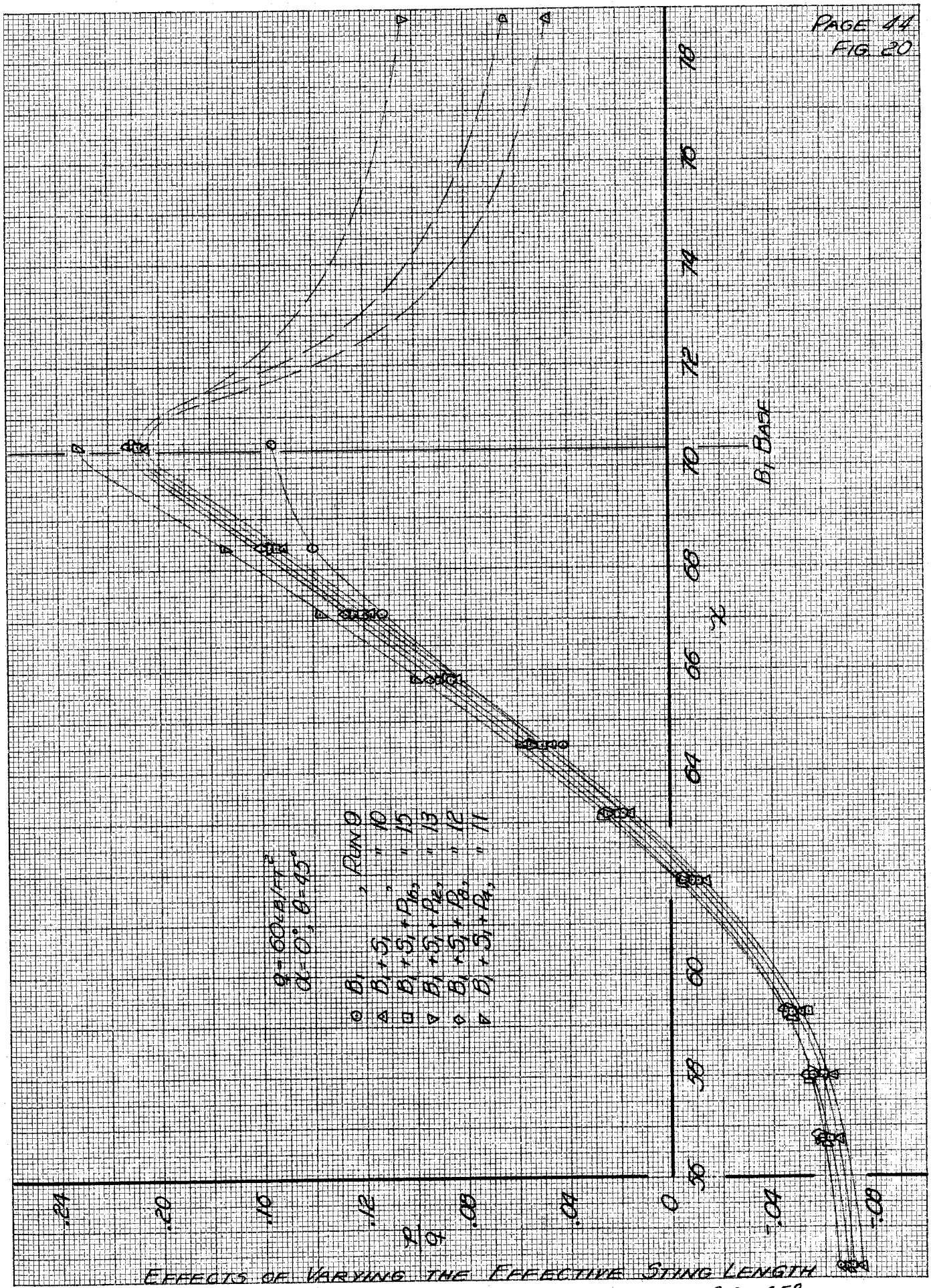

EFFECTS OF VARYING THE EFFECTIVE STING LENGTH BY THE POD, CONFIGURATION B_1, $\alpha = 0°, \theta = 45°$

C_p v.s. X

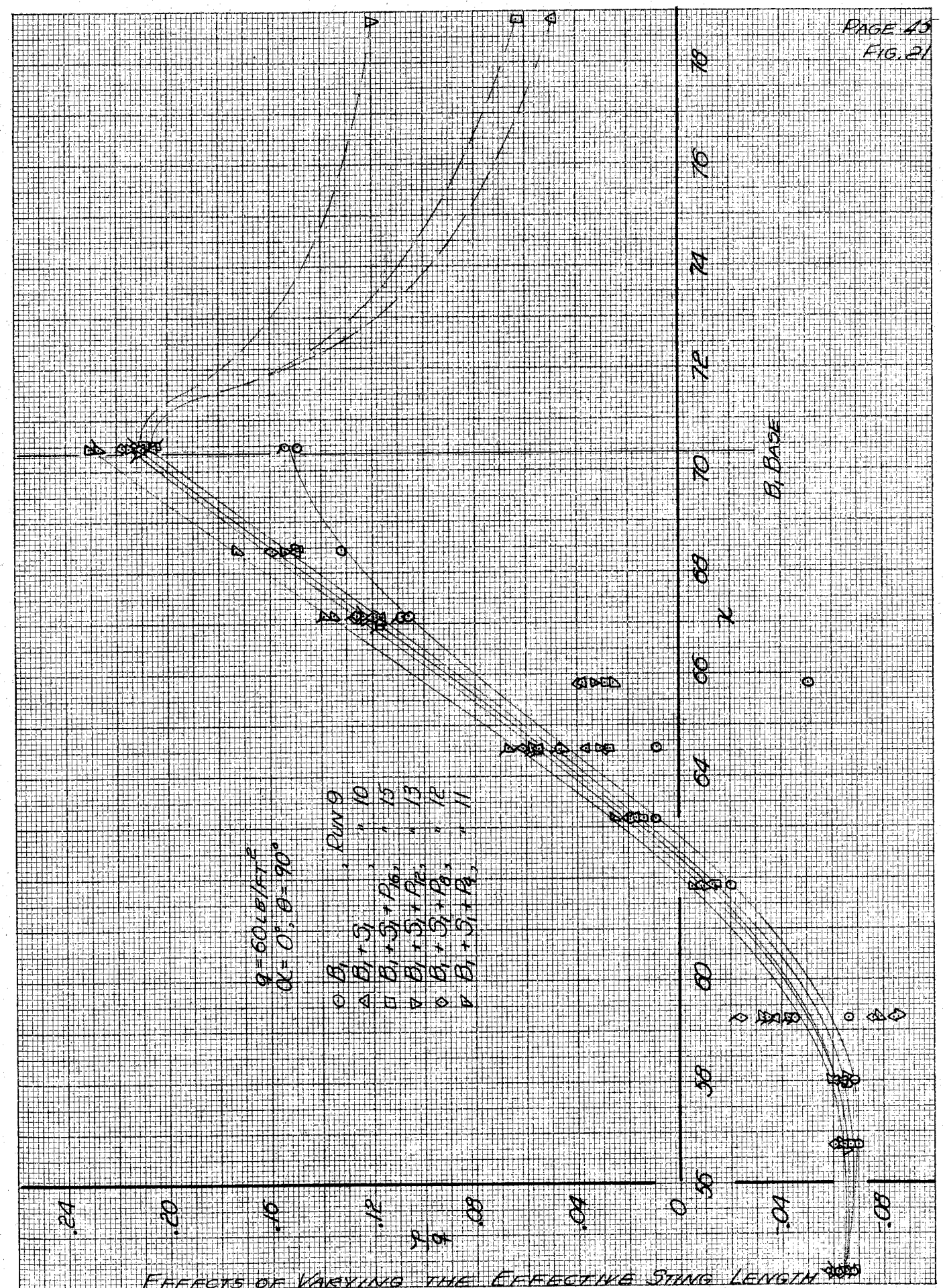

EFFECTS OF VARYING THE EFFECTIVE STING LENGTH BY THE POD, CONFIGURATION B_1, $\alpha = 0°$, $\theta = 90°$

$\bar{Y}$ VS. $\bar{X}$

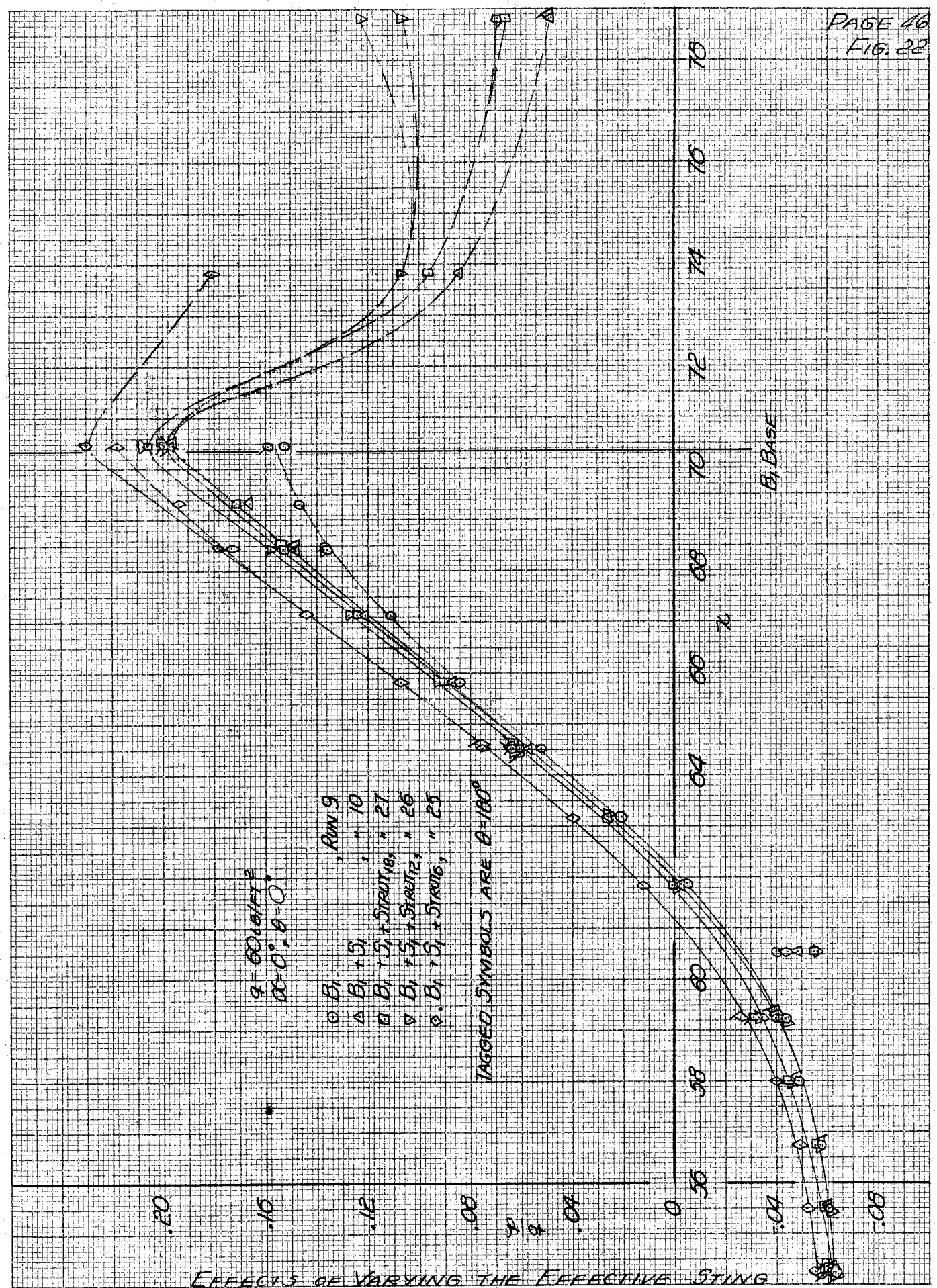

EFFECTS OF VARYING THE EFFECTIVE STING LENGTH BY THE DUMMY STRUT, CONFIGURATION B_1, $\alpha=0°$, $\theta=0°$

$\frac{p}{q}$ VS. x

FIG. 23

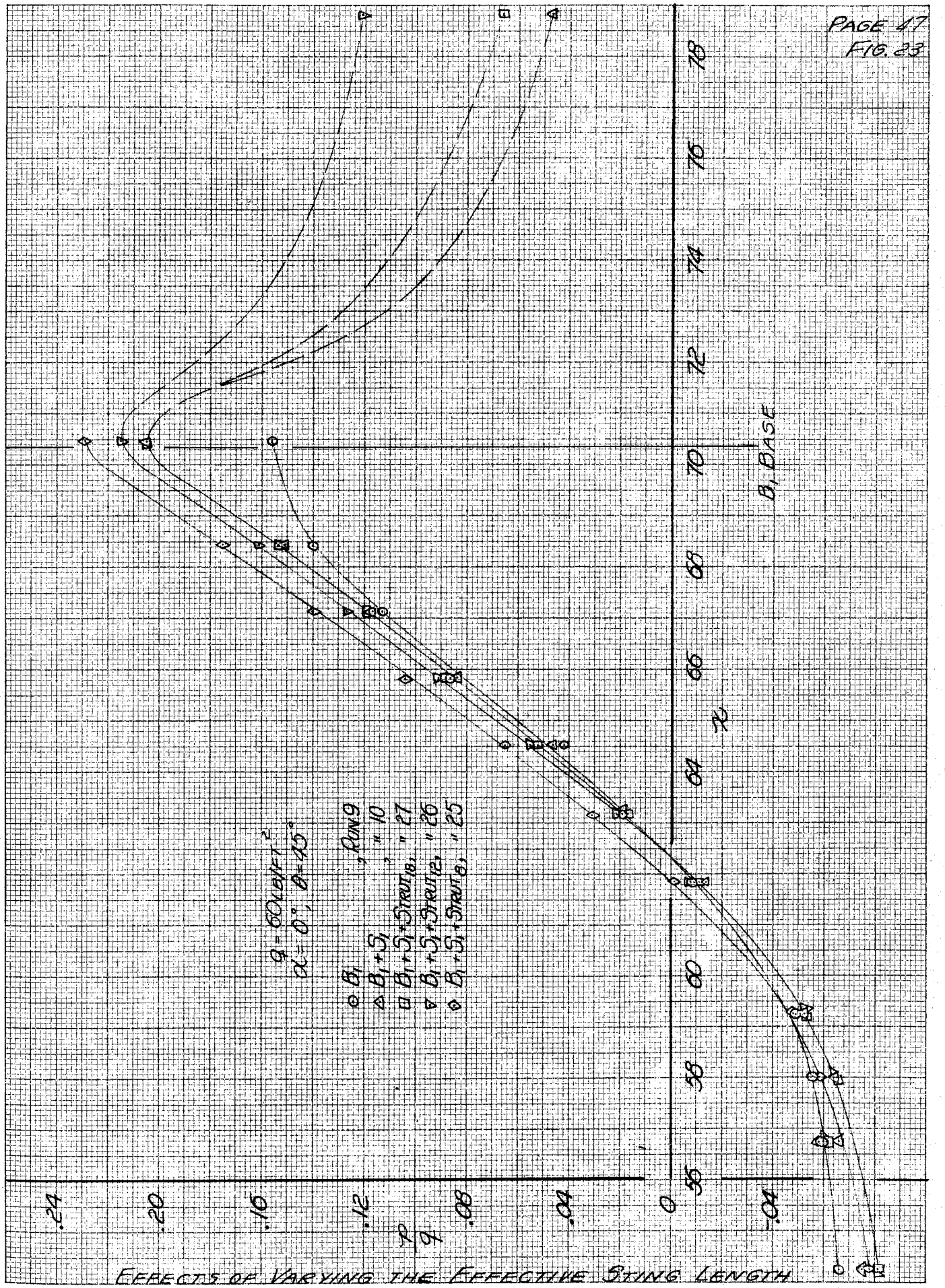

EFFECTS OF VARYING THE EFFECTIVE STING LENGTH BY THE DUMMY STRUT, CONFIGURATION B_1, $\alpha = 0°$, $\theta = 45°$

$\frac{q}{p}$ VS. x

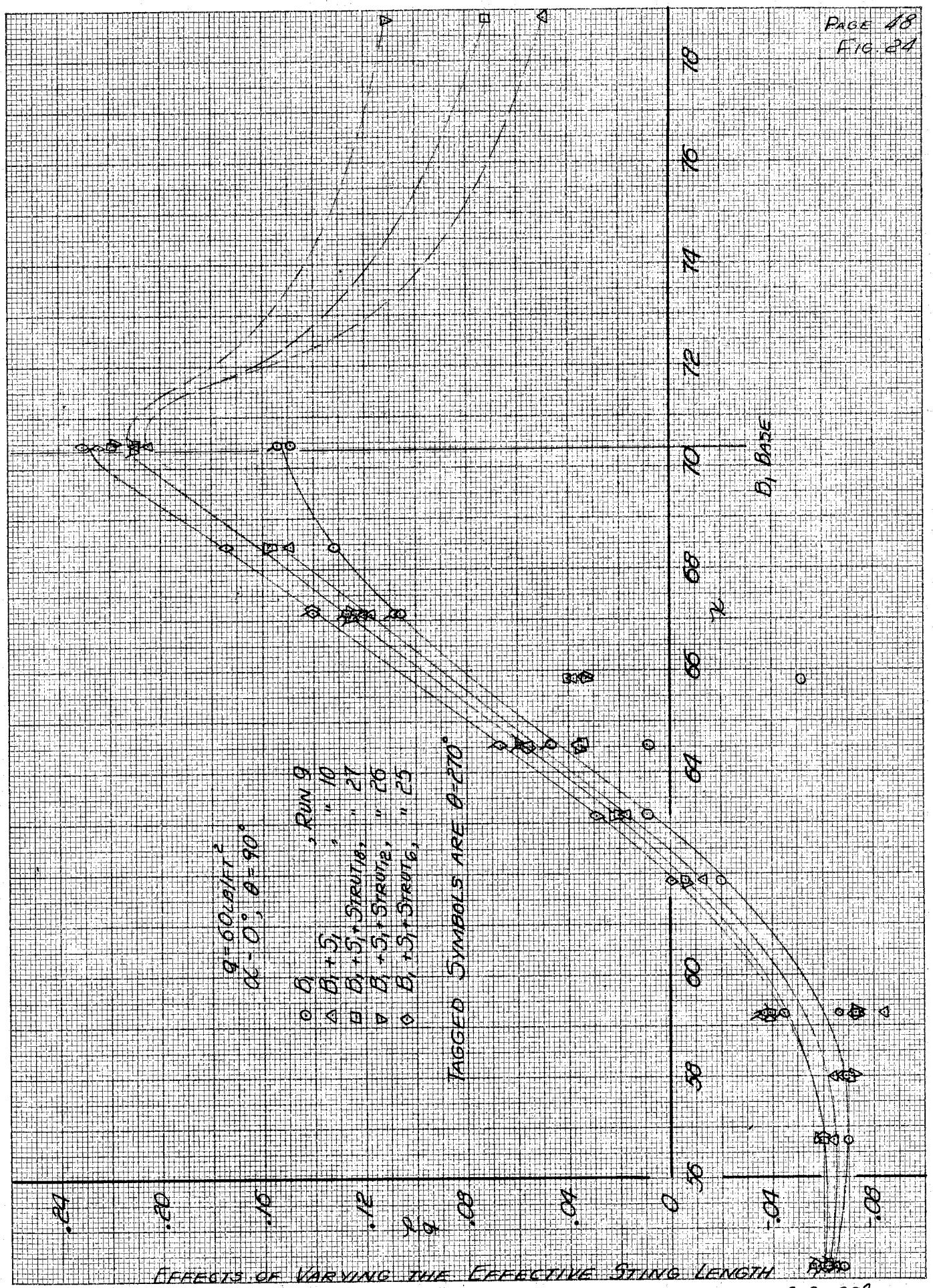

EFFECTS OF VARYING THE EFFECTIVE STING LENGTH BY THE DUMMY STRUT, CONFIGURATION B_1, $\alpha=0°$; $\theta=90°$

$\frac{P}{q}$ VS. Y

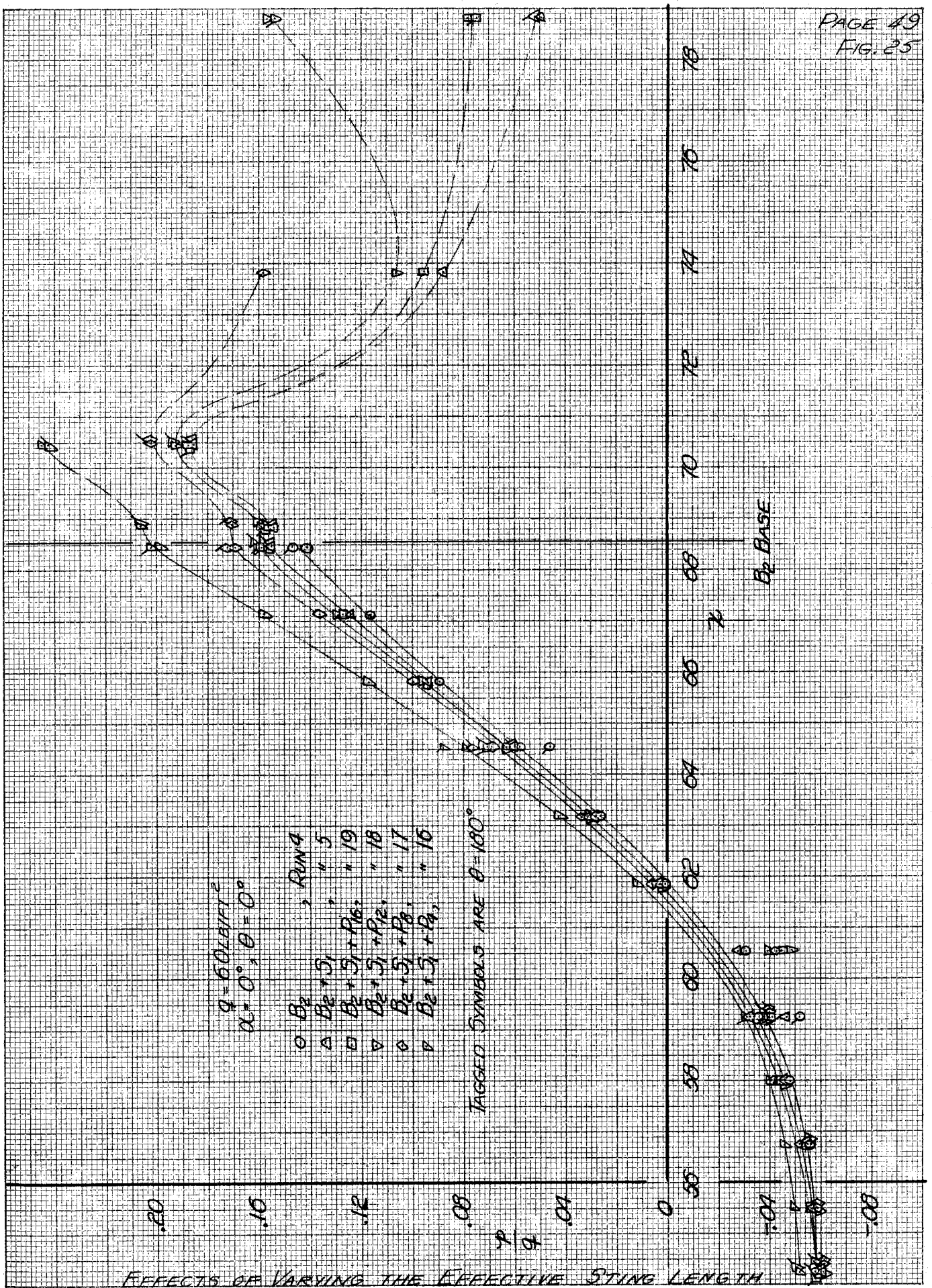

EFFECTS OF VARYING THE EFFECTIVE STING LENGTH BY THE POD, CONFIGURATION B_2, $\alpha = 0°$; $\theta = 0°$

C_Y VS. α

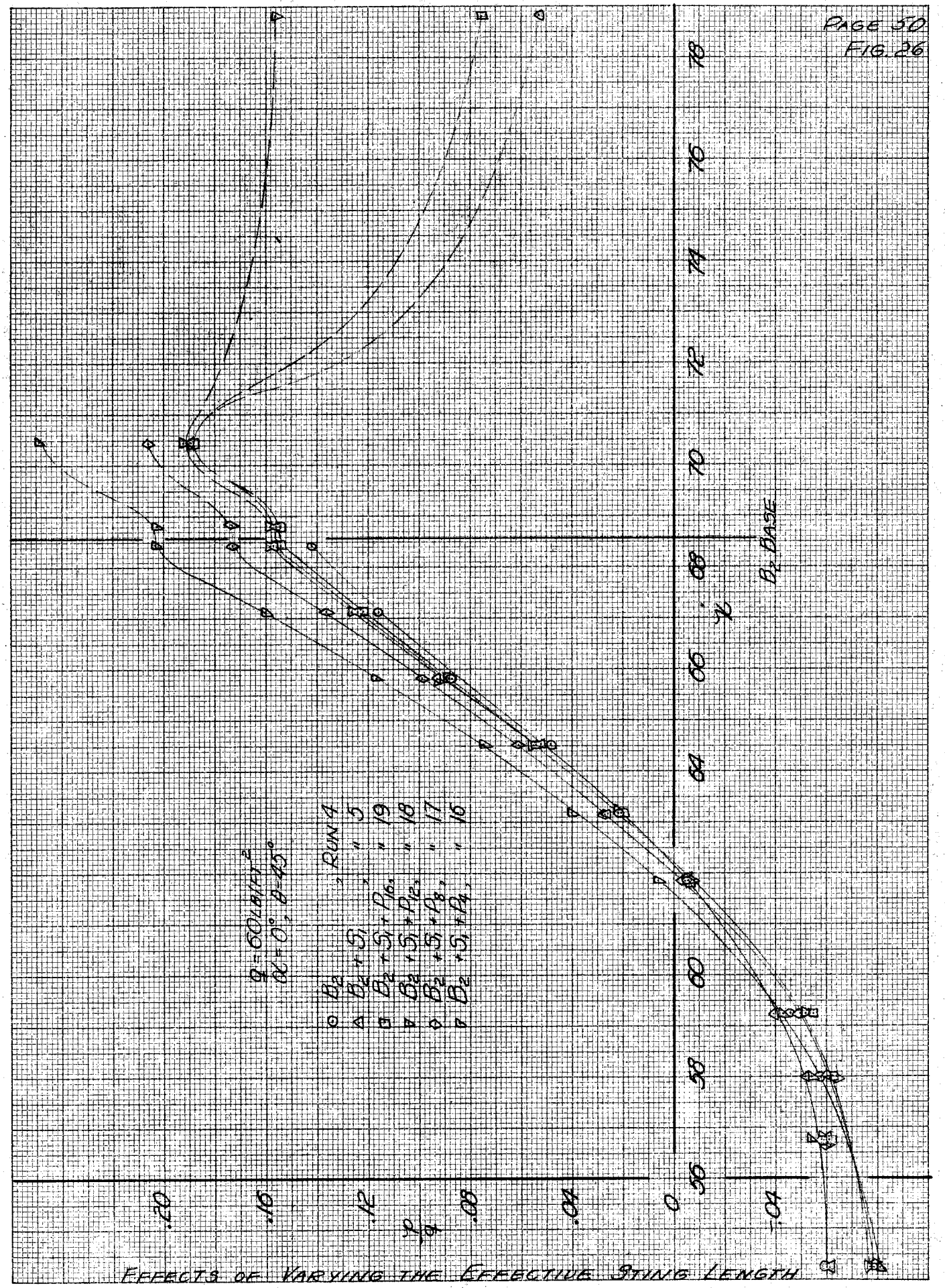

EFFECTS OF VARYING THE EFFECTIVE STING LENGTH BY THE POD, CONFIGURATION B_2, $\alpha = 0°$, $\theta = 45°$

$\frac{P}{}$ vs. ψ

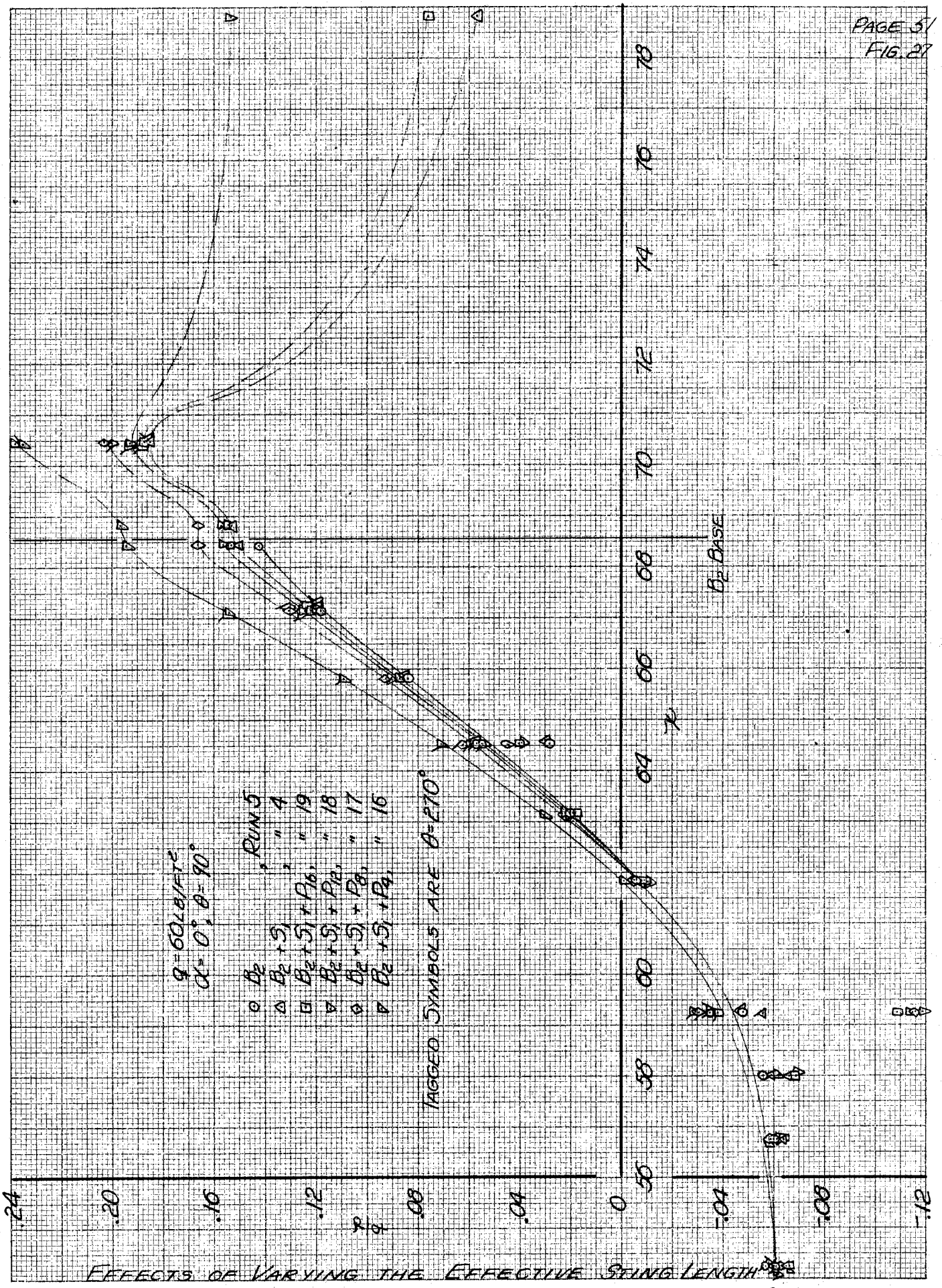

EFFECTS OF VARYING THE EFFECTIVE STING LENGTH BY THE POD, CONFIGURATION B_2, $\alpha = 0°$, $\theta = 90°$

$\frac{P}{q}$ VS. x

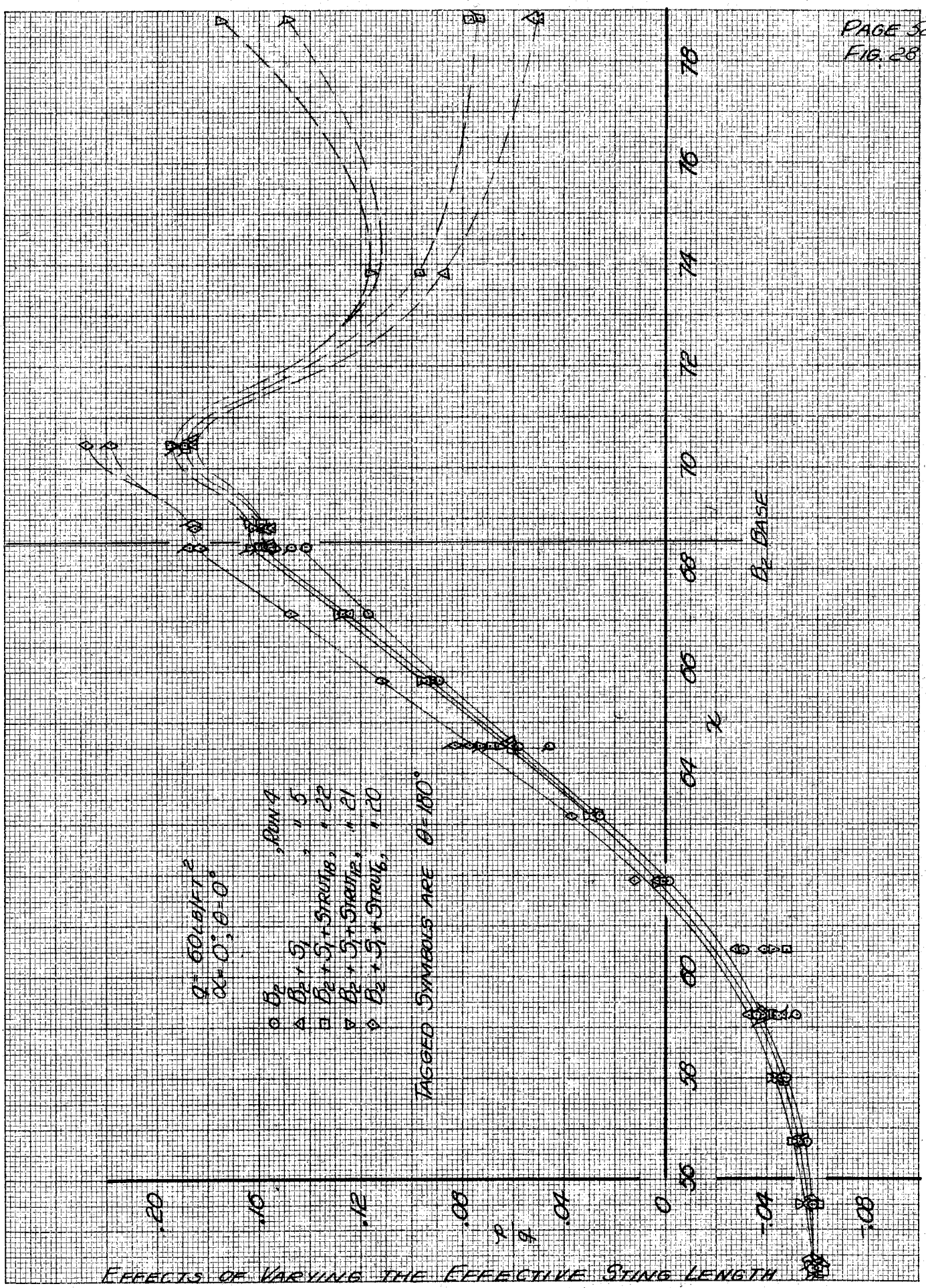

EFFECTS OF VARYING THE EFFECTIVE STING LENGTH BY THE DUMMY STRUT, CONFIGURATION B_2, $\alpha = 0°$, $\theta = 0°$

$\frac{q}{q}$ vs x

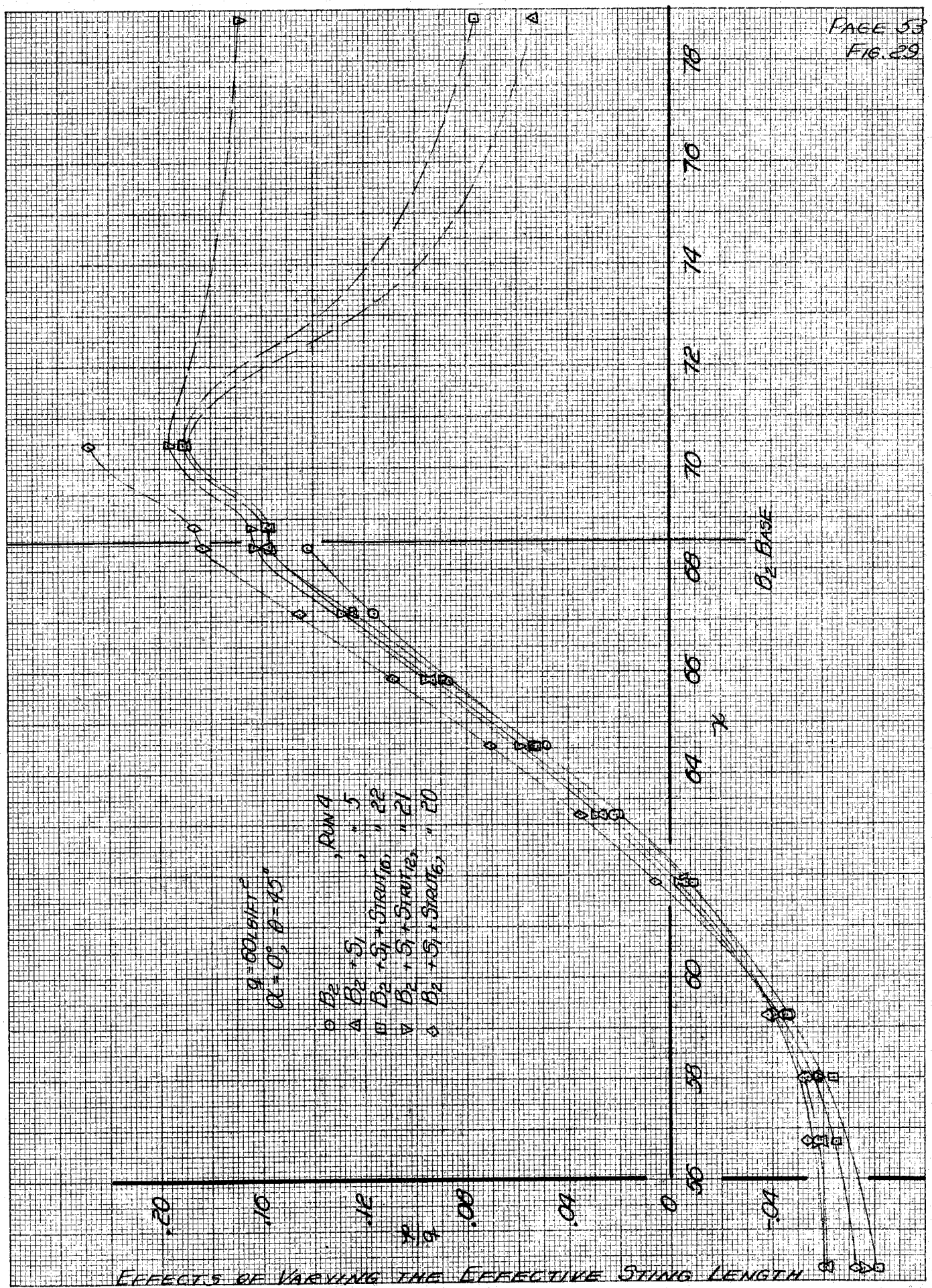

EFFECTS OF VARYING THE EFFECTIVE STING LENGTH BY THE DUMMY STRUT, CONFIGURATION B_2, $\alpha = 0°$, $\theta = 45°$

χ VS. χ

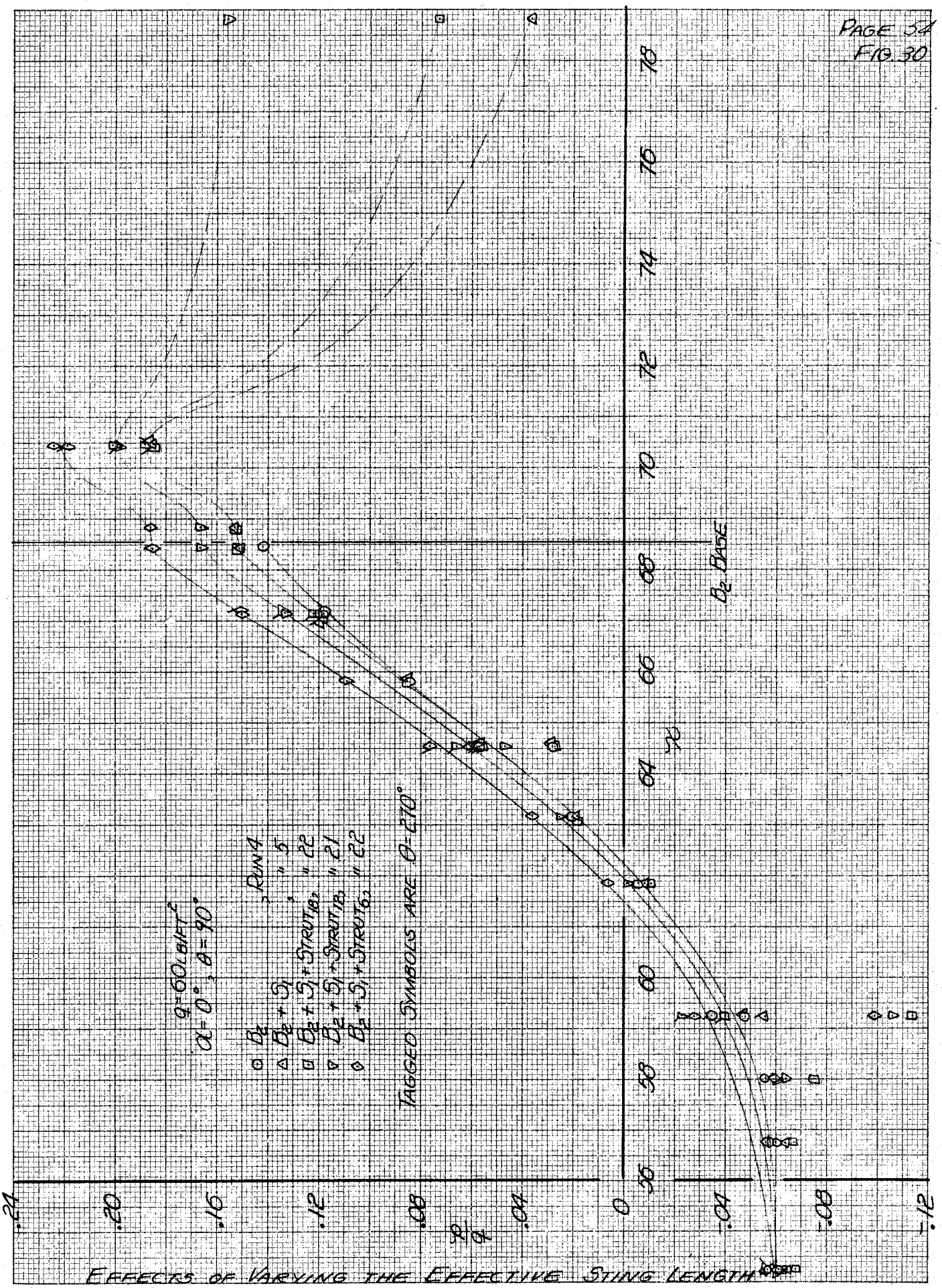

Effects of Varying the Effective Sting Length by the Dummy Strut, Configuration B_2, $\alpha = 0°$, $\theta = 90°$

C_L vs. x

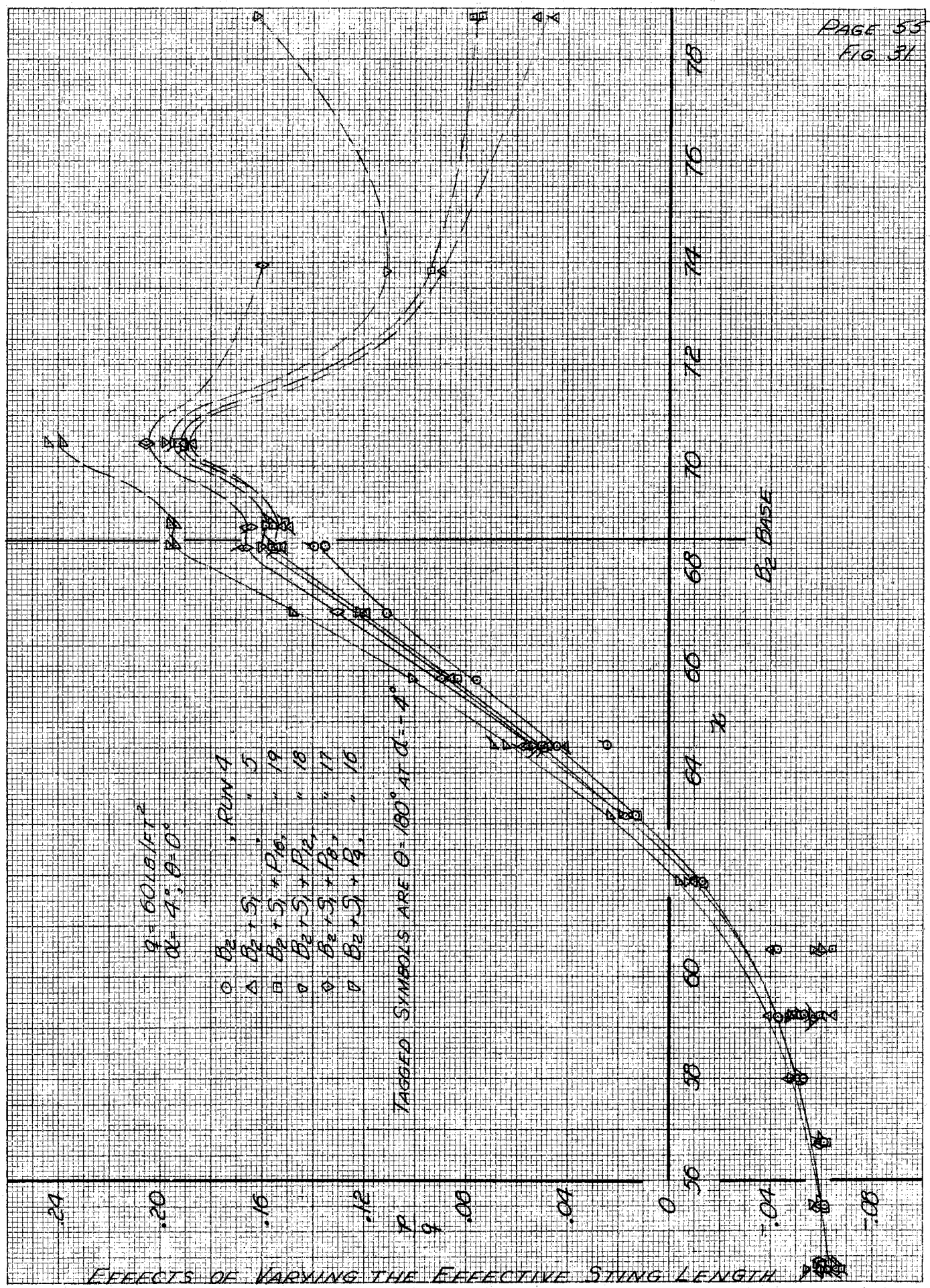

EFFECTS OF VARYING THE EFFECTIVE STING LENGTH BY THE POD, CONFIGURATION B_2, $\alpha = 4°$, $\theta = 0°$

$\frac{p}{q}$ VS. x

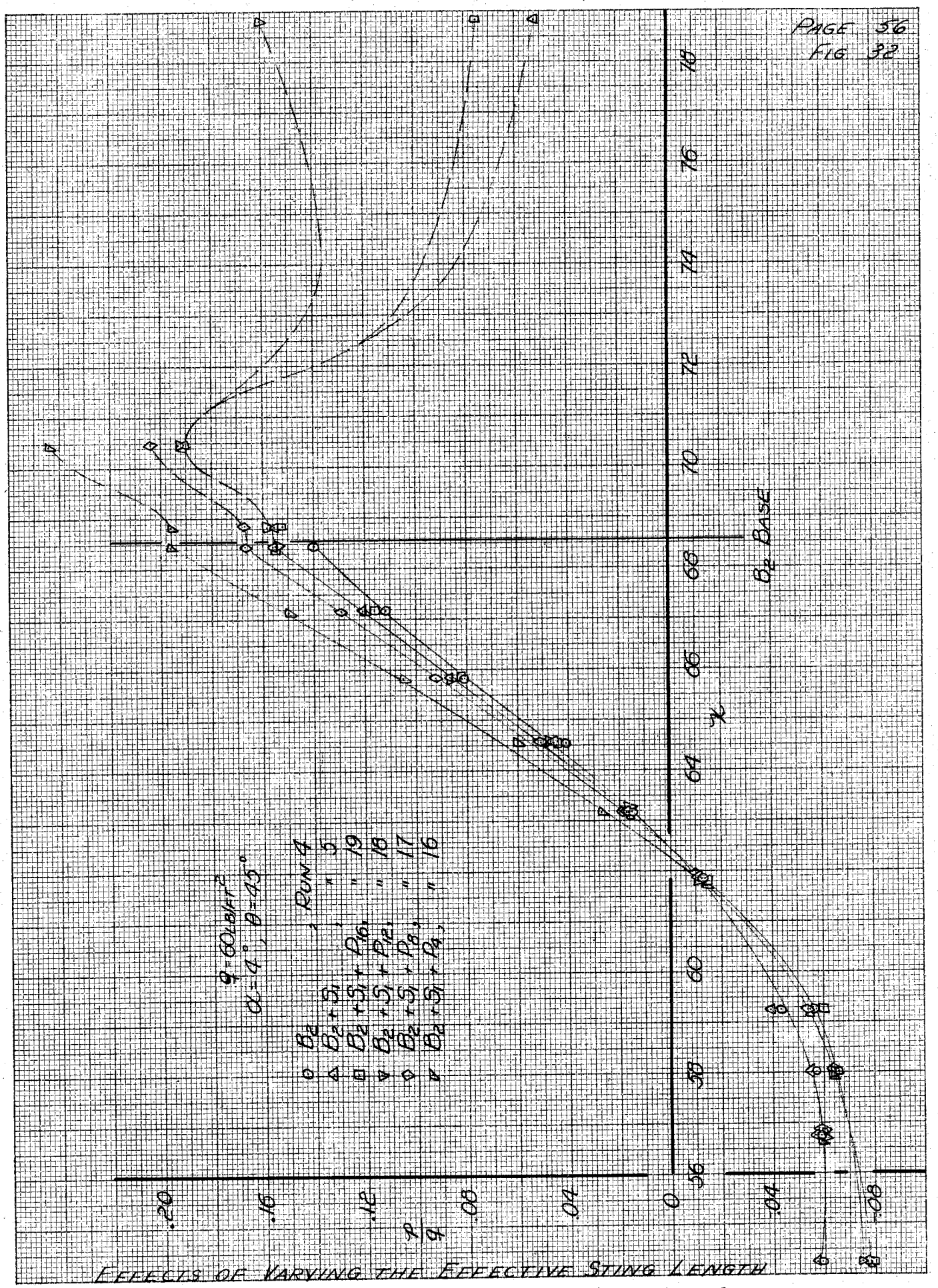

EFFECTS OF VARYING THE EFFECTIVE STING LENGTH BY THE POD, CONFIGURATION B_2, $\alpha = 4°$, $\theta = 45°$

$\frac{R}{q}$ VS. χ

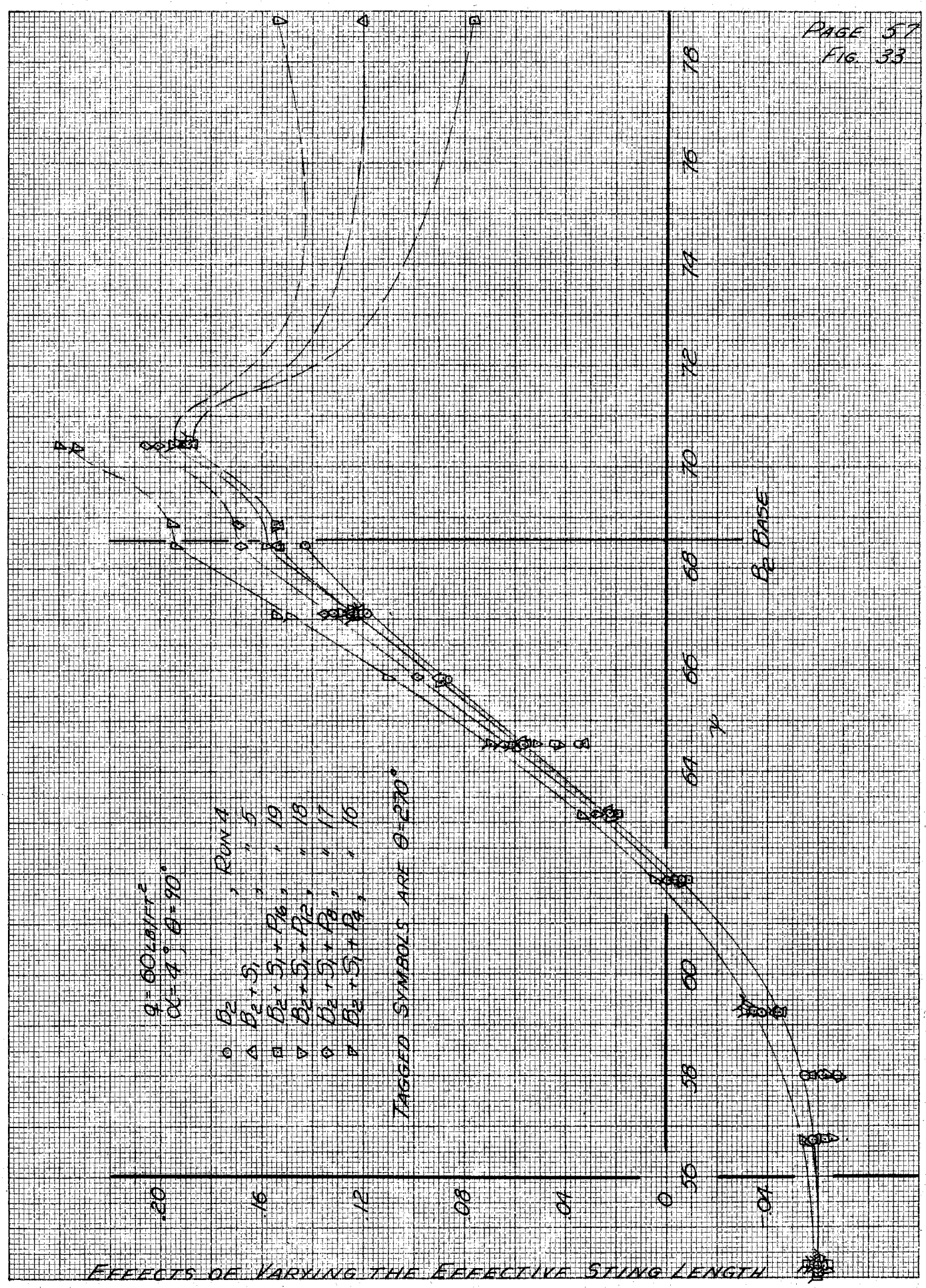

EFFECTS OF VARYING THE EFFECTIVE STING LENGTH BY THE POD, CONFIGURATION B_2, $\alpha = 4°$, $\theta = 90°$

$\frac{p}{q}$ VS. x

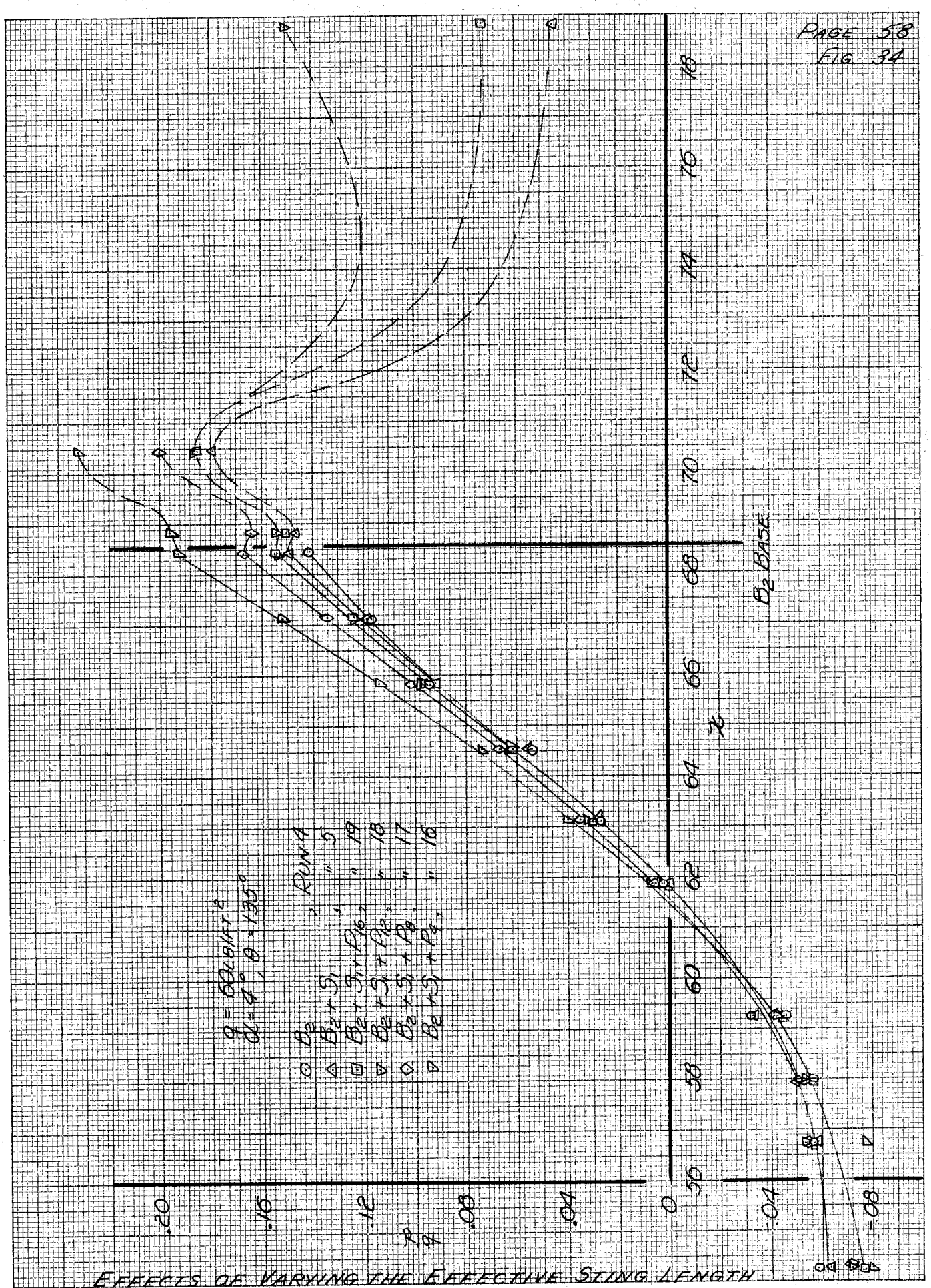

EFFECTS OF VARYING THE EFFECTIVE STING LENGTH BY THE POD, CONFIGURATION B_2, $\alpha = 4°$, $\theta = 135°$

$\frac{p}{q}$ VS. x

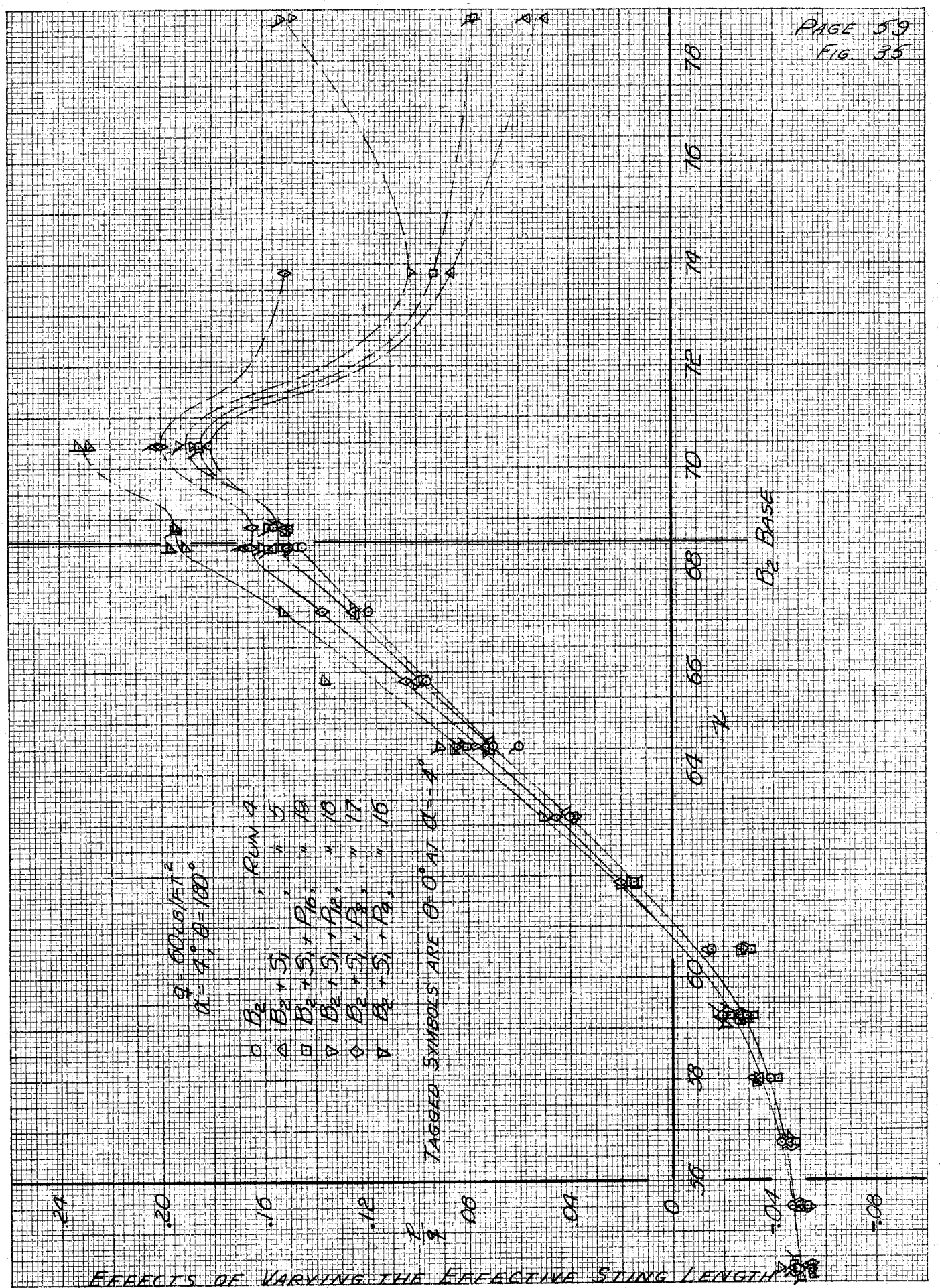

EFFECTS OF VARYING THE EFFECTIVE STING LENGTH BY THE POD, CONFIGURATION B_2, $\alpha = 4°$, $\theta = 180°$

$\frac{p}{q}$ VS. x

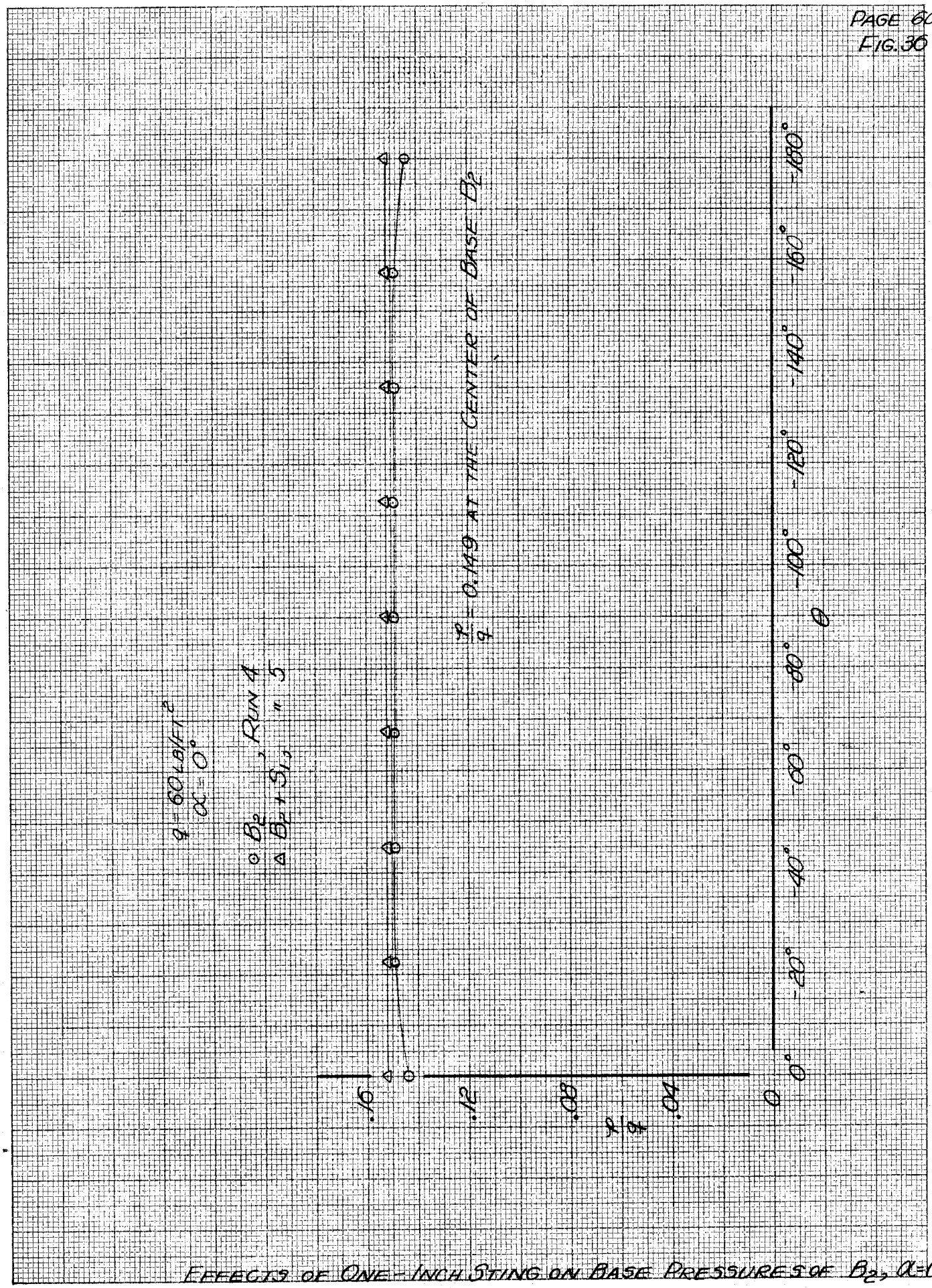

EFFECTS OF ONE-INCH STING ON BASE PRESSURES OF B_2, $\alpha = 0°$

$\frac{p}{q}$ vs. θ

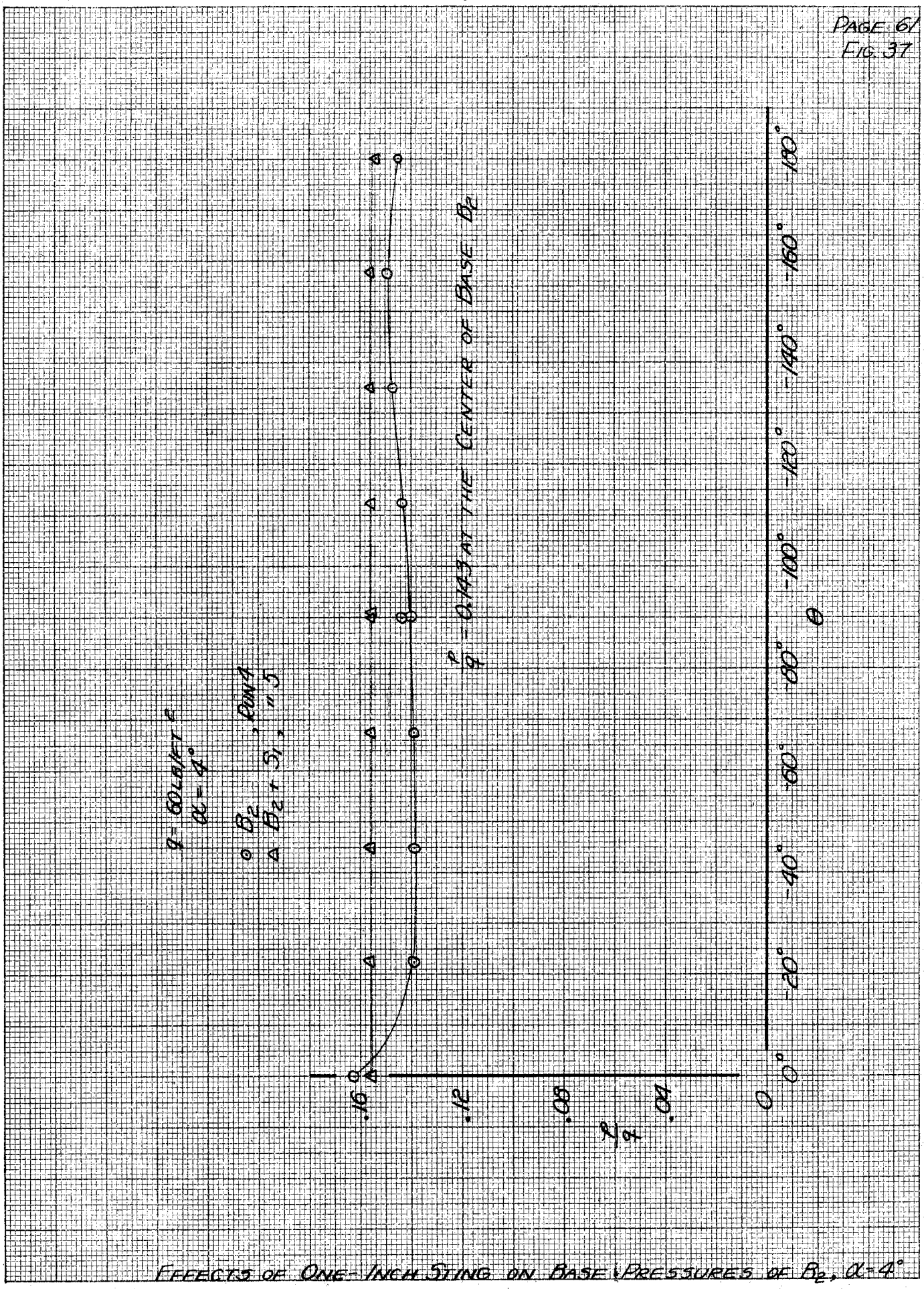

EFFECTS OF ONE-INCH STING ON BASE PRESSURES OF B_2, $\alpha = 4°$

$\frac{P}{q}$ VS. θ

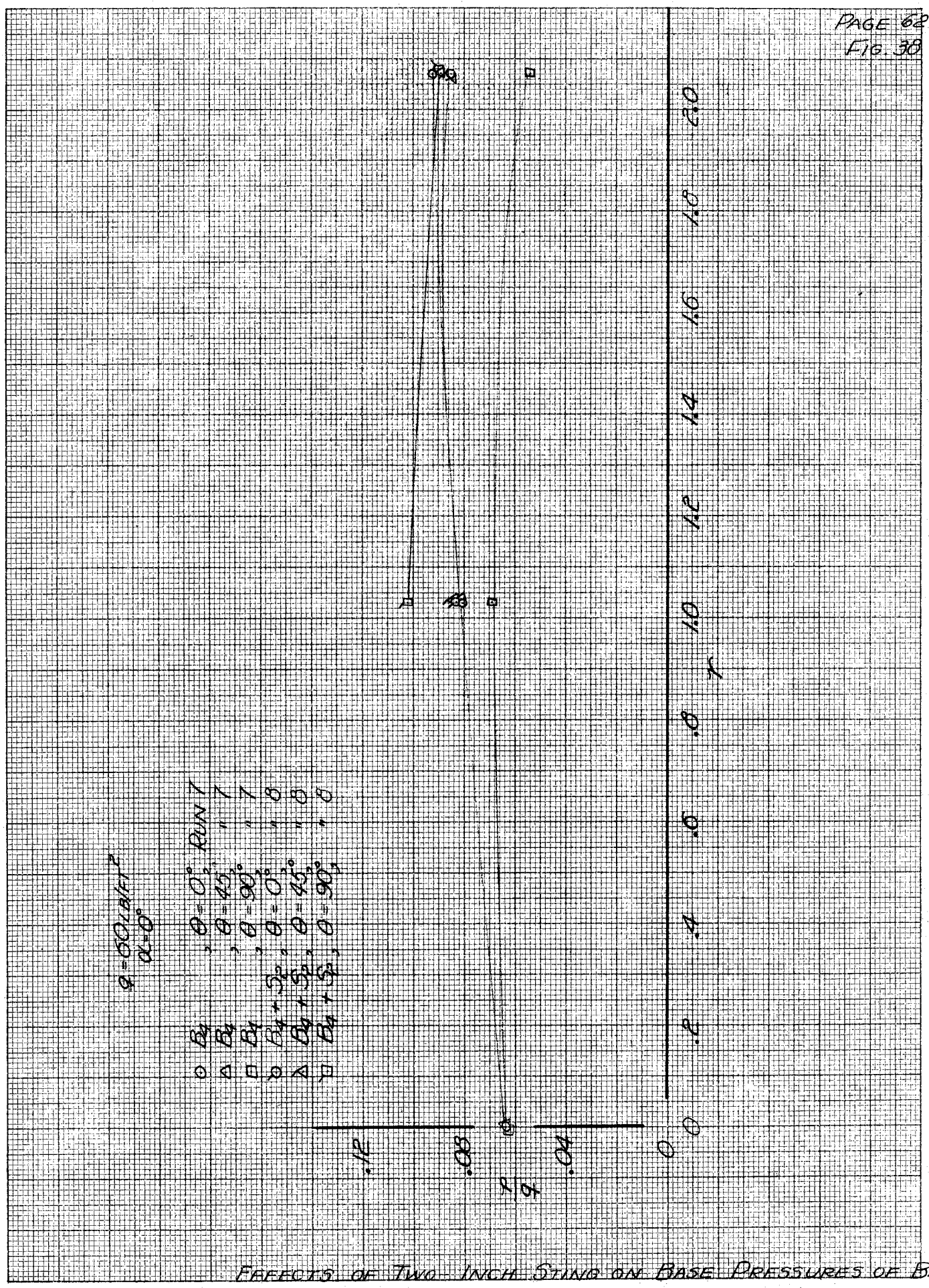

EFFECTS OF TWO INCH STING ON BASE PRESSURES OF B_4,
$\alpha = 0°$
p VS. r

EFFECTS OF STING LENGTH ON BASE PRESSURES OF B_2, $\alpha = 0°$

$\frac{p}{q}$ VS. Y

FIG. 40

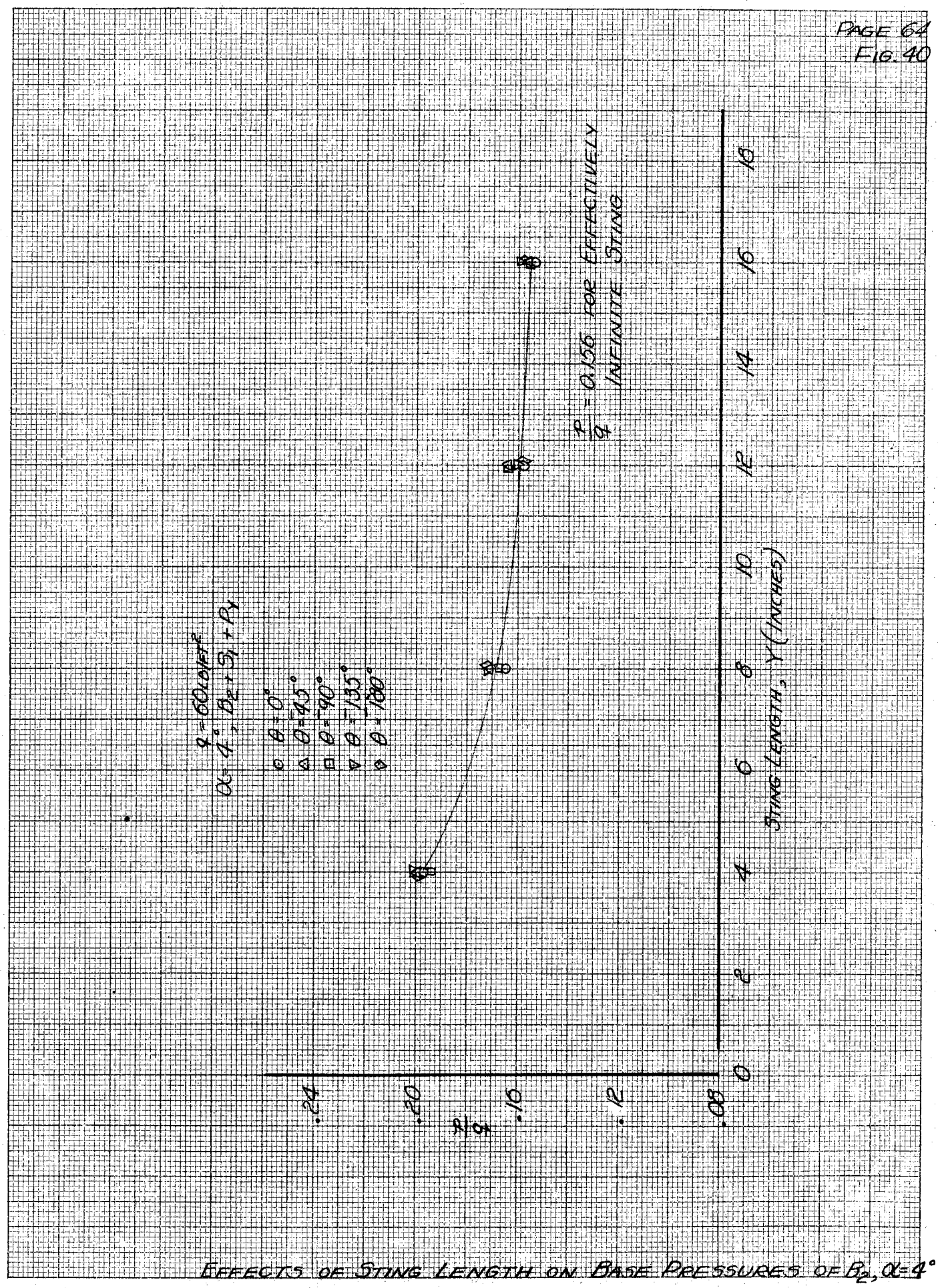

EFFECTS OF STING LENGTH ON BASE PRESSURES OF B_2, $\alpha = 4°$

$\frac{P}{Q}$ VS. Y

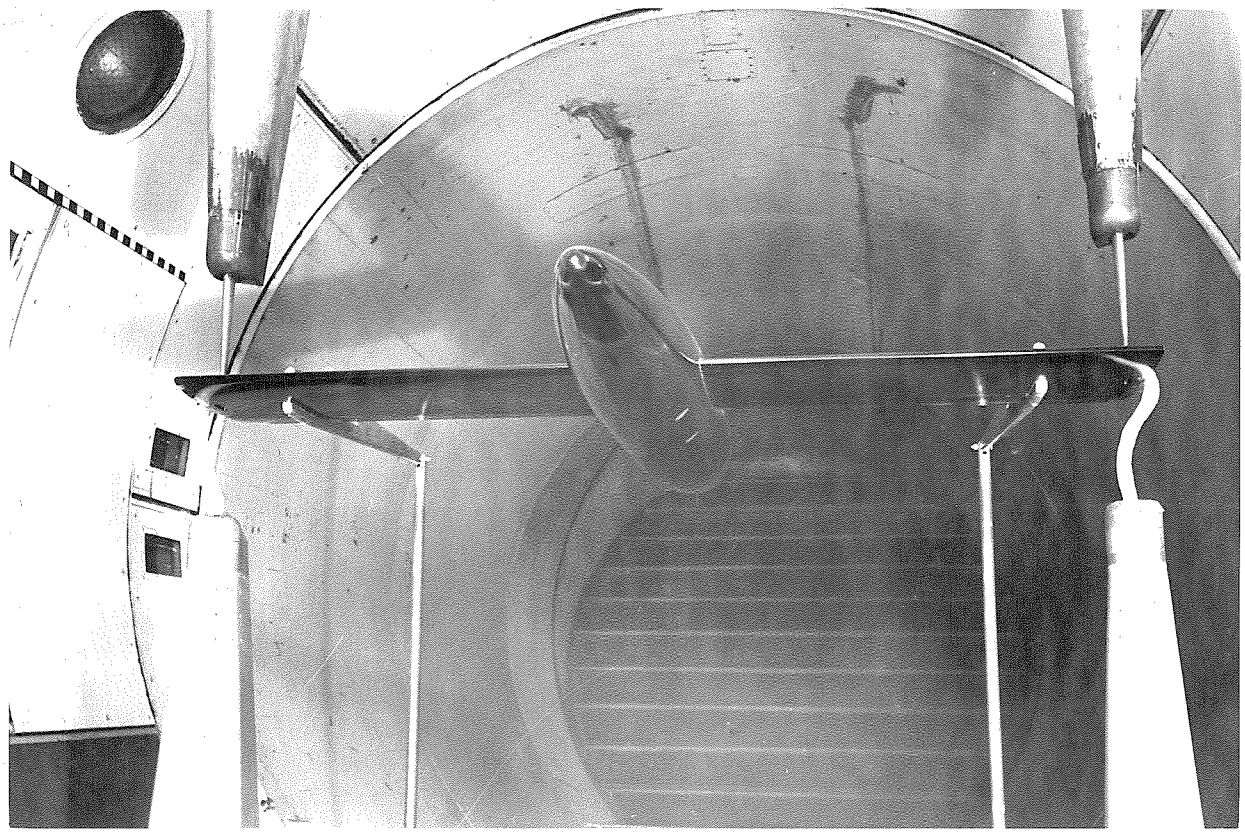

Photo 1. Lower-front view of configuration B showing the model installed in the tunnel

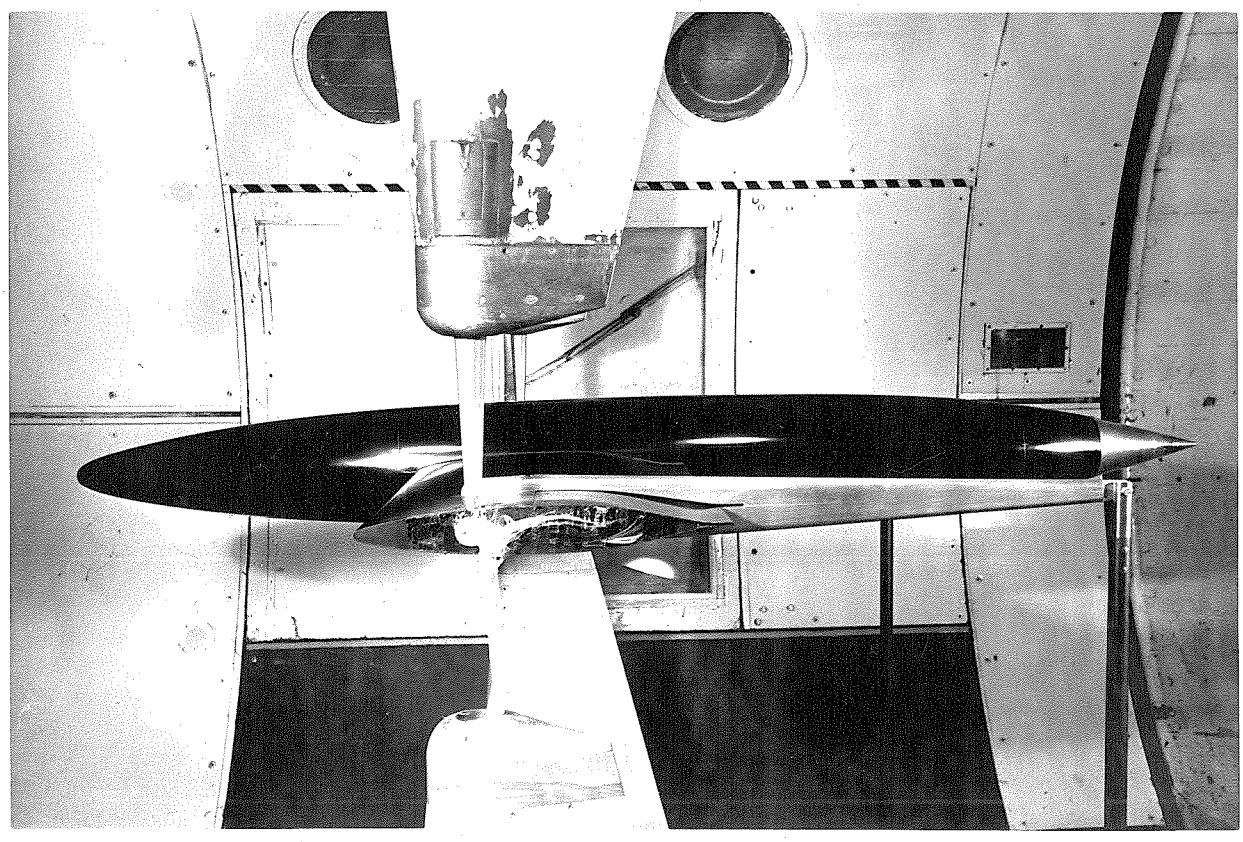

Photo 2. Side view of configuration B

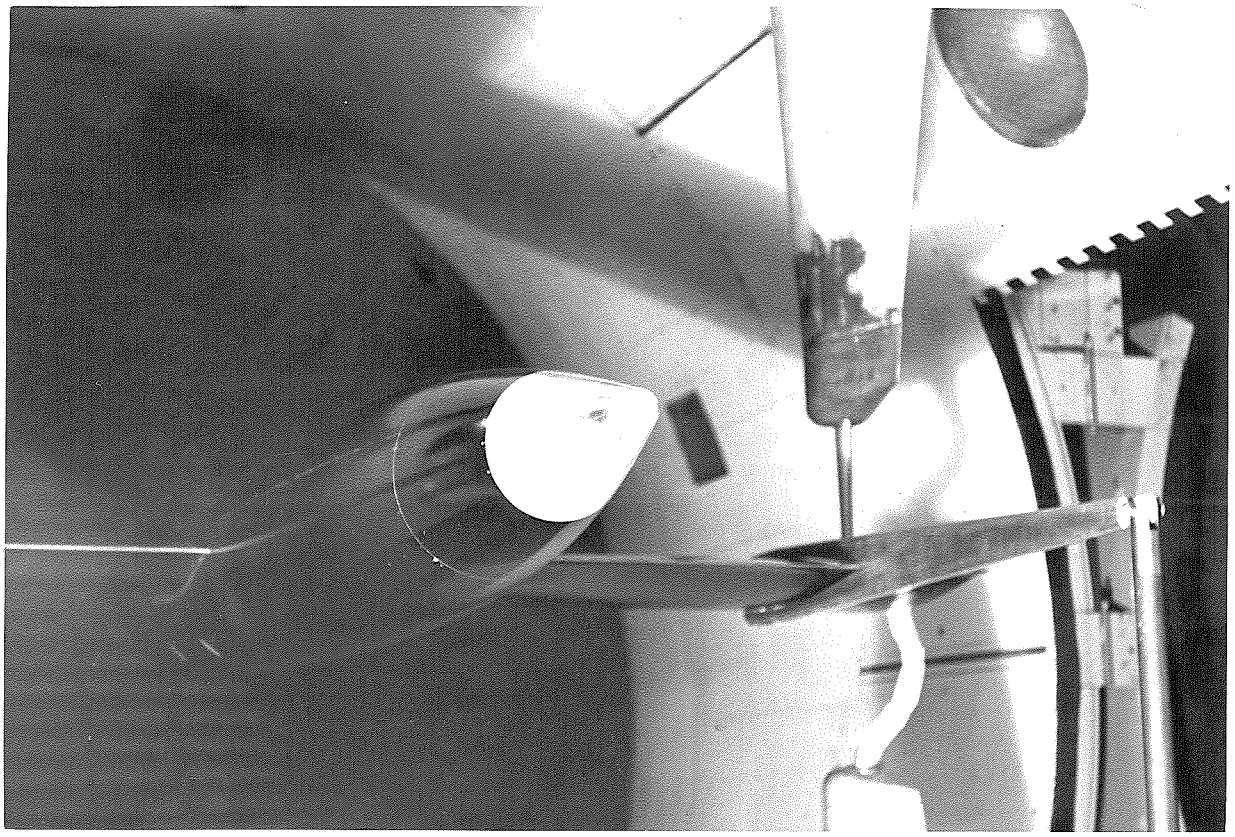

Photo 3. Rear view of configuration B_1

Photo 4. Rear-side view of configuration $B_1 + S_1$

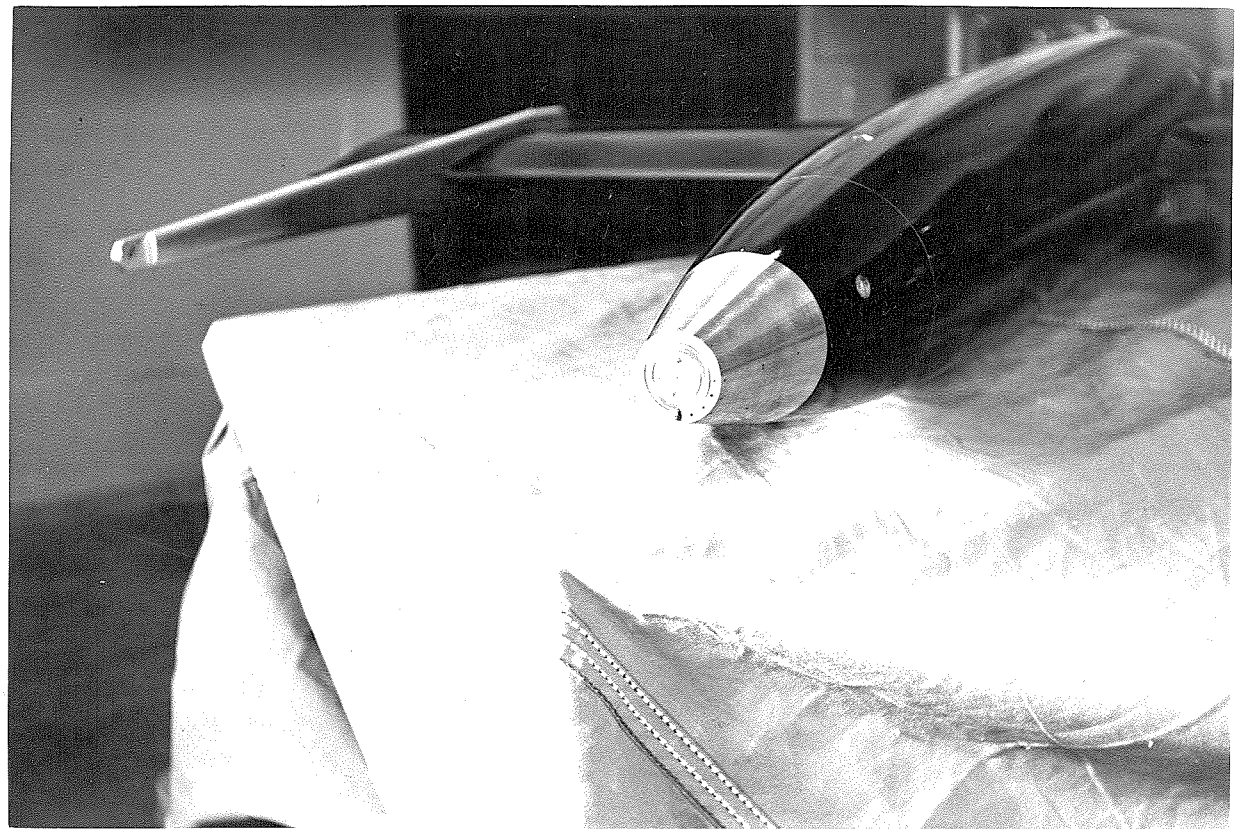

Photo 5. Rear-side view of configuration B_2 showing base pressure orifices

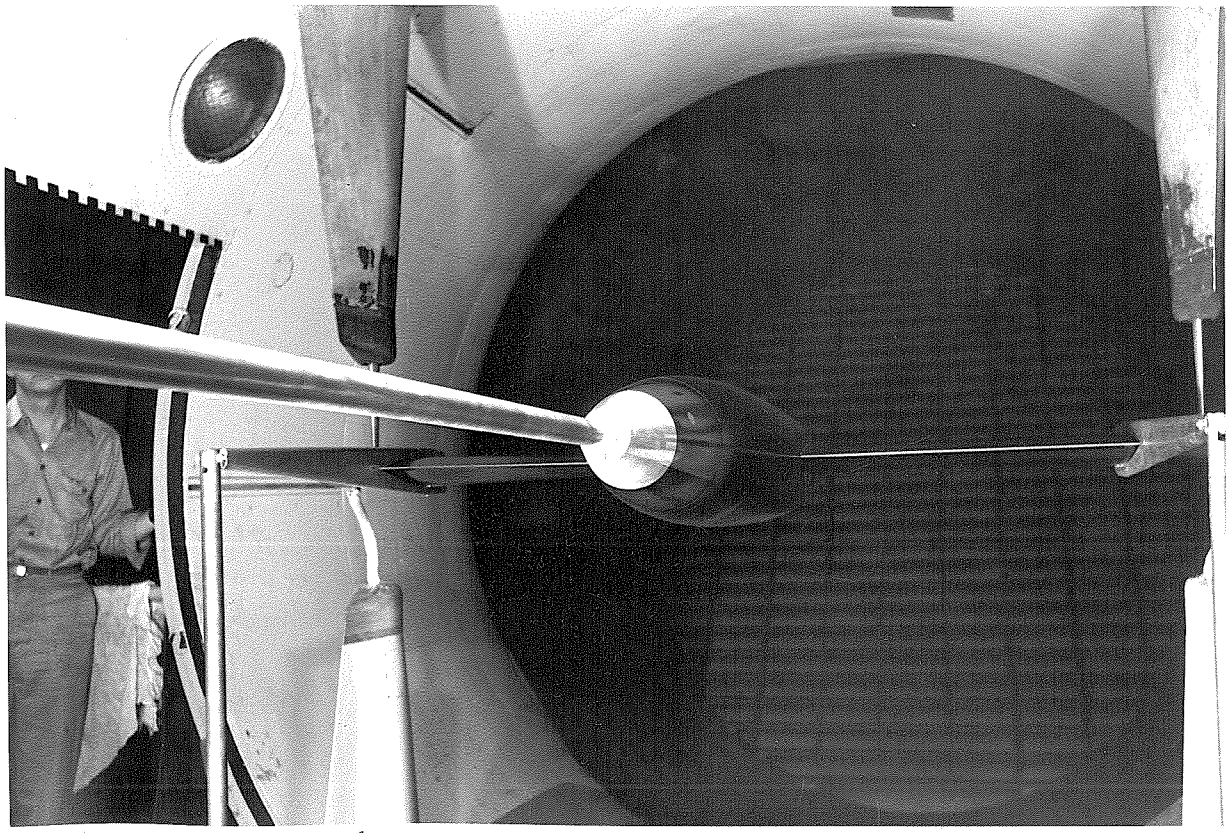

Photo 6. Rear-side view of configuration $B_2 + S_1$

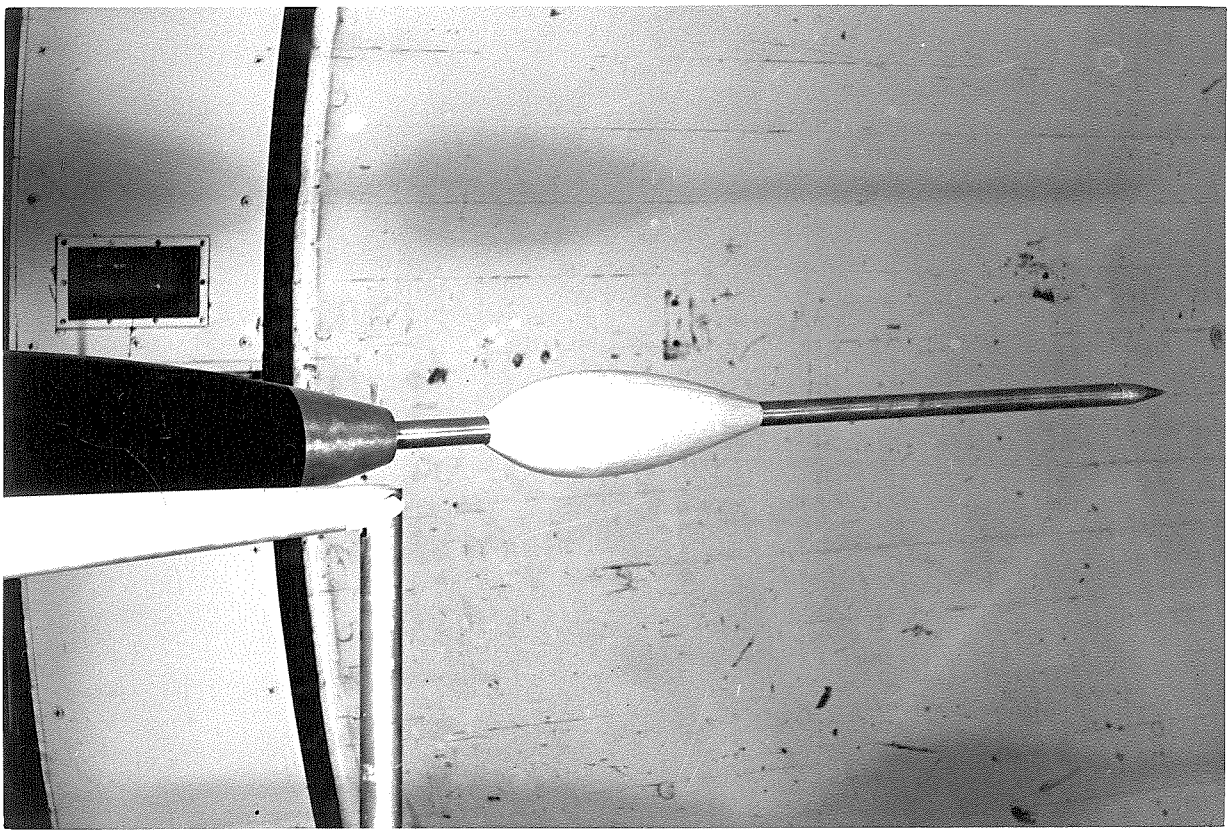

Photo 7. Side view of configuration $B_2 + S_1 + P_4$ showing pod

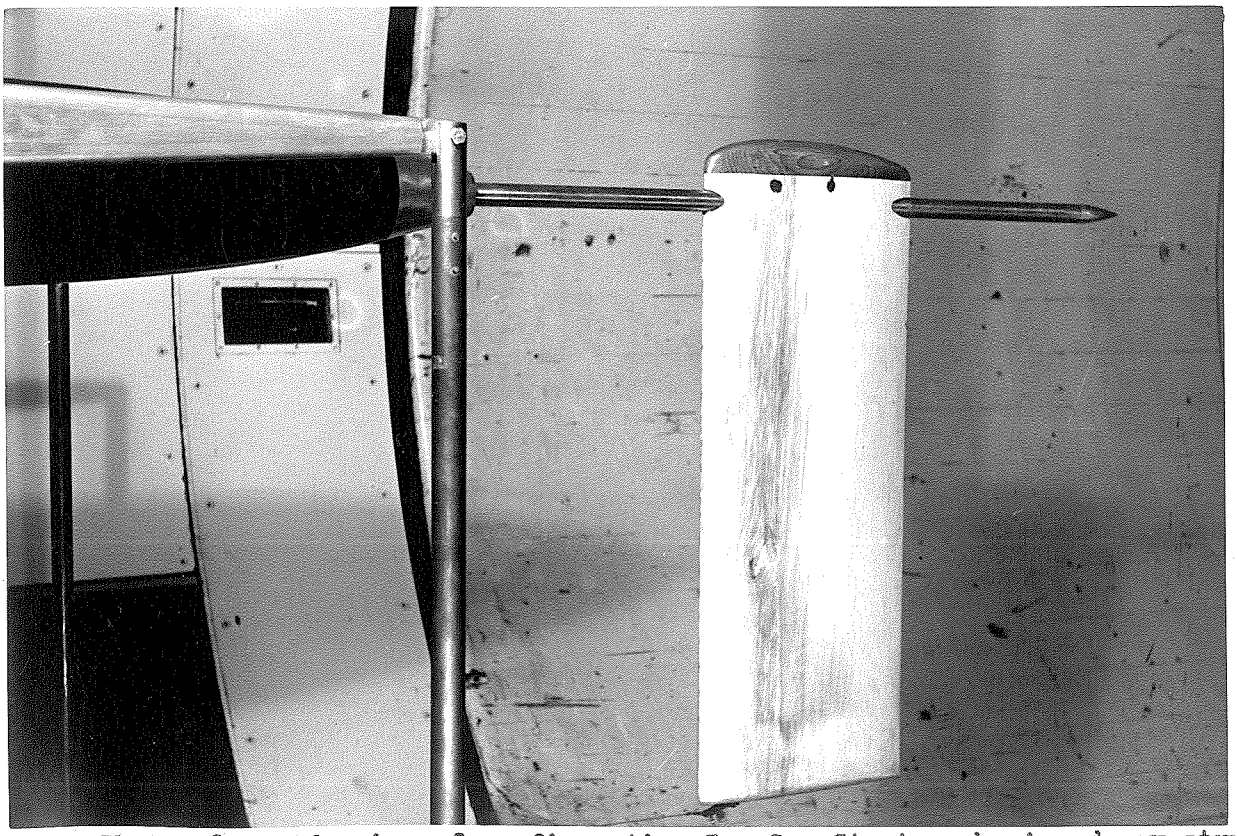

Photo 8. Side view of configuration $B_2 + S_1 + Strut_{12}$ showing dummy strut

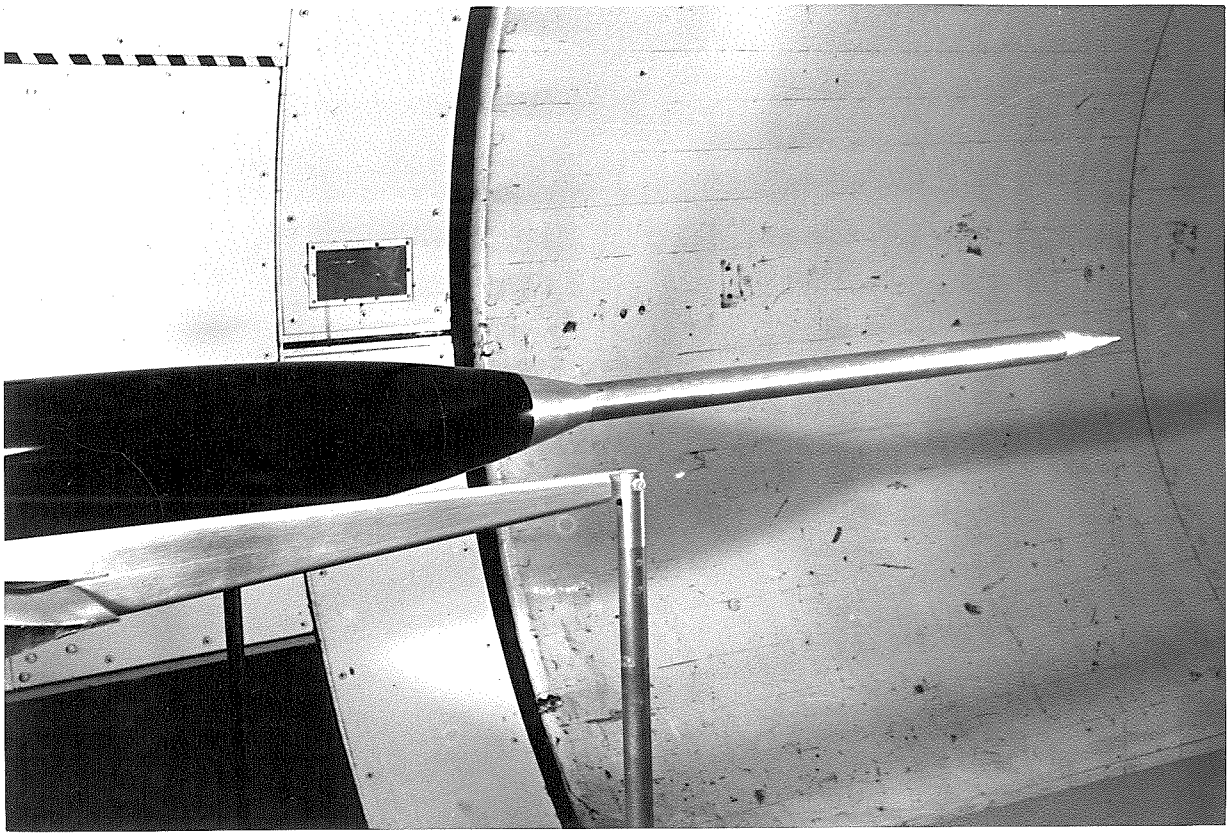

Photo 9. Side view of configuration $B_2 + S_2$ showing the effective infinite sting

Photo 10. Rear view of configuration B_4 showing base pressure orifices

Photo 11. Rear view of configuration B_4+S_2

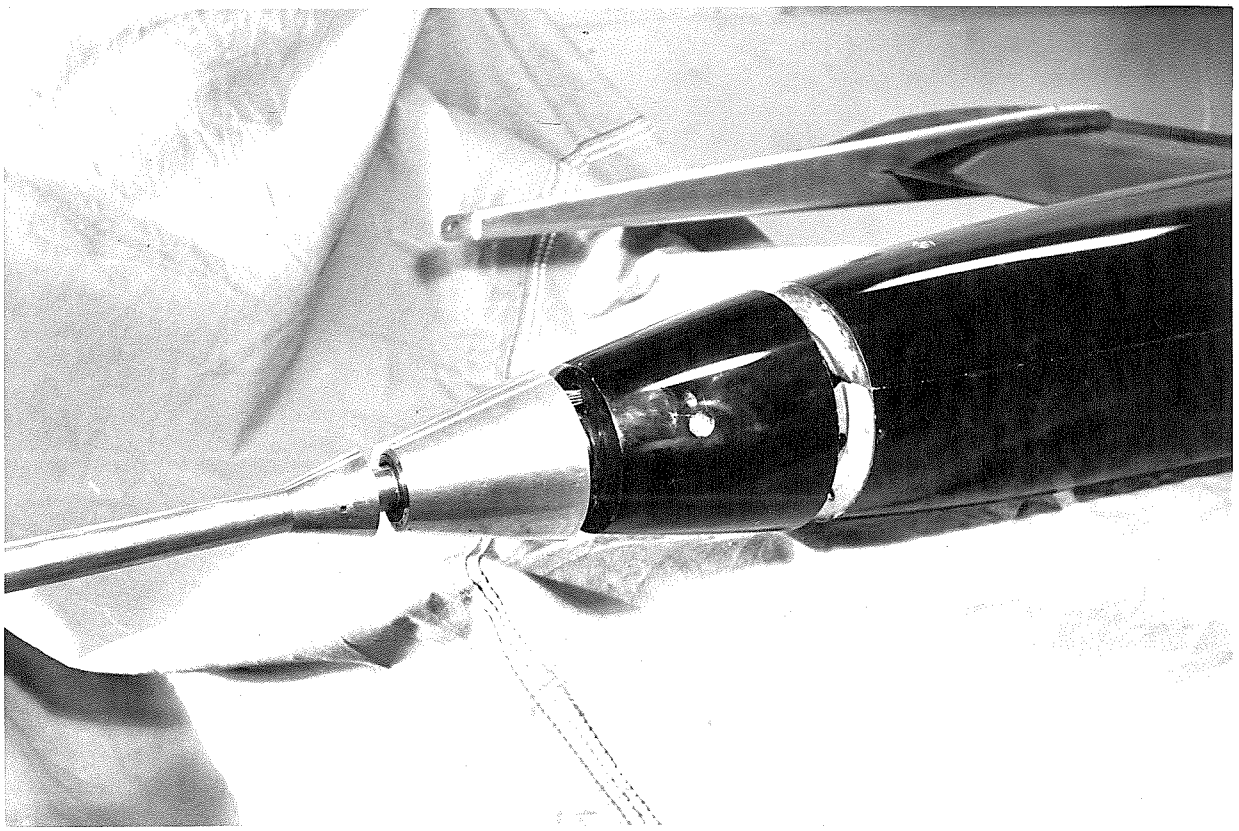

Photo 12. Configuration $B_1 + S_1$ showing removable aft sections

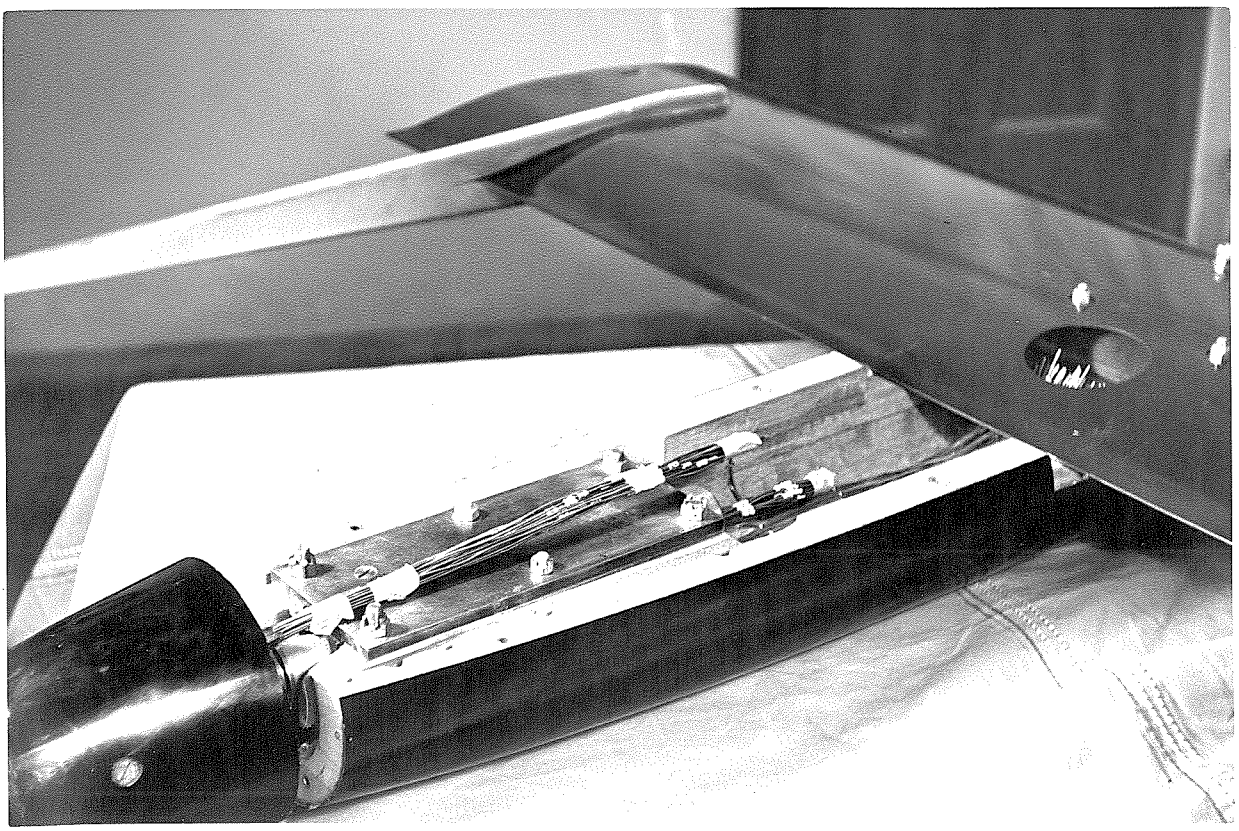

Photo 13. Photo showing the pressure leads inside the fuselage